UCSF

UC San Francisco Electronic Theses and Dissertations

Title

Structural basis for catalytic activity and regulation of isocitrate dehydrogenase

Permalink

https://escholarship.org/uc/item/769991pf

Author

Hurley, James H.

Publication Date

1990

Peer reviewed|Thesis/dissertation

eScholarship.org Powered by the California Digital Library
University of California

Structural Basis for Catalytic Activity and Regulation of Isocitrate Dehydrogenase

by

James H. Hurley

DISSERTATION

Submitted in partial satisfaction of the requirements for the degree of

DOCTOR OF PHILOSOPHY

in

Biophysics

in the

GRADUATE DIVISION

of the

UNIVERSITY OF CALIFORNIA

San Francisco

Approved:

Robert M Stroud March 21st 1990
Robert Fletterick March 23, 1990
Daniel E. Koshland Jr. April 14, 1990

Committee in Charge

Deposited in the Library, University of California, San Francisco

[redacted]

Copyright (1990)
by
James H. Hurley

except Chapter 3,
Copyright (1990)
by
The Journal of Biological Chemistry

Preface

It is an axiom of modern biochemistry that structure determines function. By understanding the relationship between macromolecular structures and their functions we can make the connection between the precise laws of physics and chemistry and the bewilderingly complex properties of living things. This thesis describes the elucidation of the structural basis for both the catalytic activity and regulation of an enzyme, isocitrate dehydrogenase, by means of the most powerful experimental methodology available: x-ray crystallography. Many testable predictions have been made based on the structural analysis, some with the aid of electrostatic potential calculations, and a way has been opened for much further analysis of structure and function of isocitrate dehydrogenase by site-directed mutagenesis, theoretical calculations, and x-ray crystallography.

The introduction to this thesis summarizes the background for work described in detail in the manuscripts which make up subsequent chapters. Chapter 2 appeared in the Proceedings of the National Academy of Sciences (1989) **86**:8635-8639, chapter 3 appeared in the Journal of Biological Chemistry (1990) **265**:3599-3602 and is reproduced by permission, and chapters 4 and 5 will be submitted for publication.

Many colleagues, both in the macromolecular structure group at UCSF and in Dan Koshland's lab at UC Berkeley, have provided valuable contributions to this work. The work of Nancy Helmers and Peter Thorsness

led to the crystallization of isocitrate dehydrogenase (IDH), without which the structural studies would have been possible. Joe Day, Eric Fauman, V. Ramalingam, and Julie Sohl have all been involved in the IDH project, and the work of Antony Dean has been particularly important in the later stages of this project. The IDH project is a collaboration with the laboratory of Daniel E. Koshland, Jr., whose group established the regulatory role of phosphorylation of IDH, and has had a central role in the elucidation of its regulatory mechanism. Specific acknowledgements are found within individual chapters.

I would like to thank my colleagues Celia Schiffer, Partho Ghosh, Stephanie Mel, Janet Finer-Moore, Bill Montfort, Kathy Perry, Cynthia Wolberger, Michael Shuster, Thomas Earnest, Alok Mitra, Larry Miercke, Susan Fong, Sally Raguet, and Amir Attaran for insightful crystallographic discussions and/or making the Stroud lab a fun place to be. I thank Mel Jones, Dave Herrmann, and Angus McDonald for keeping the x-ray instruments and computers going, and Julie Ransom, the biophysics program administrator and foster mother to biophysics students. Professors Robert Fletterick and Peter Kollman in the biophysics group at UCSF have made particularly important contributions to my education, inspiring a continuing interest in using computer simulations based on physical principles to make the connection between macromolecular structure and function. A fellowship from the U. C. Regents provided the bulk of the financial support for my Ph. D. studies.

Above all, I thank my advisor and friend, Bob Stroud, who has taught me much about how to do science, and more about why to do science: for the fun of it.

Abstract

Structural Basis for Catalytic Activity and Regulation of Isocitrate Dehydrogenase

by

James H. Hurley

Isocitrate dehydrogenase catalyzes the oxidation of isocitrate to α-ketoglutarate by $NAD(P)^+$, a step in the citric acid cycle, the principal cycle responsible for extraction of energy from fats and carbohydrates in aerobic metabolism. X-ray crystallography has been used to investigate the mechanisms of regulation and catalysis of isocitrate dehydrogenase, and to explore the evolution of this enzyme. The structure of the free enzyme, solved by the isomorphous replacement method, showed no nucleotide-binding fold typical of other dehydrogenases, indicating a distinct evolutionary history from most other dehydrogenases.

The isocitrate dehydrogenase of *Escherichia coli* is regulated by phosphorylation at serine 113, which inactivates the enzyme by preventing isocitrate binding. Phosphorylated isocitrate dehydrogenase undergoes minimal structural changes compared to the dephosphorylated enzyme, and structures of inactive site-directed mutants at residue 113 show essentially no structural changes. In the complex with Mg^{++} isocitrate, the γ-carboxylate of isocitrate is hydrogen bonded to serine 113. Electrostatic calculations with the Poisson-Boltzmann equation show that introduction of negative charge at residue 113 has a large effect on the electrostatic component of the free energy of binding of isocitrate. Inactivation is thus mediated by a combination of direct steric and electrostatic interactions with the substrate, not by conformational changes in the enzyme.

A catalytic mechanism for isocitrate dehydrogenase has been inferred based on the crystallographic structure of Mg^{++} isocitrate bound to the enzyme and kinetic and spectroscopic data. Mg^{++}, coordinated by the α-carboxylate and hydroxyl oxygen of isocitrate, is an electrostatic catalyst in both the dehydrogenation and decarboxylation steps of the reaction. Aspartate 283' (on the second subunit) is probably the base involved in the dehydrogenation step, and either tyrosine 160 or lysine 230' is probably the acid which protonates the enolate form of α-ketoglutarate after decarboxylation. The residues interacting with Mg^{++}, α- and β-carboxylates, and the hydroxyl oxygen are identical in the aligned sequences of isopropylmalate dehydrogenase, indicating a common evolutionary origin and catalytic mechanism for these functionally similar enzymes.

Table of Contents

PAGE

Copyright ii

Preface iii

Abstract v

Table of Contents viii

Chapter 1: Introduction 1

Chapter 2: Structure of a Bacterial Enzyme Regulated by Phosphorylation, Isocitrate Dehydrogenase 8

Chapter 3: Regulation of Isocitrate Dehydrogenase by Phosphorylation Involves No Long-range Conformational Change in the Free Enzyme 37

Chapter 4: Phosphorylation of an Enzyme at the Active Site 56

Chapter 5: Catalytic Mechanism of Isocitrate Dehydrogenase: Structure of a Ternary Mg^{++} Isocitrate Complex 80

Chapter 6: Conclusion 109

Introduction

The citric acid cycle (Fig. 1) is at the center of aerobic metabolism. Acetyl groups from the oxidation of carbohydrates and fatty acids are further oxidized to carbon dioxide by nicotinamide adenine nucleotide cofactors, which then transfer electrons to the oxidative phosphorylation apparatus and ultimately provide the energy source for the synthesis of ATP.

Isocitrate dehydrogenase (IDH) catalyzes one of the major energy-extracting steps of this cycle, the oxidation of isocitrate to α-ketoglutarate by $NAD(P)^+$ (Fig. 2). In eukaryotes, a mitochondrial NAD^+-dependent IDH is active in the citric acid cycle, and a distinct $NADP^+$-dependent IDH has a biosynthetic role. In prokaryotes, $NADP^+$-dependent IDH predominates and is active in the citric acid cycle. The $NADP^+$-dependent IDHs from prokaryotes and eukaryotes are similar kinetically and share the same requirement for divalent cations, while the eukaryotic NAD^+-dependent IDH does not require divalent cations and is probably unrelated to $NADP^+$-dependent IDH. The IDH step of the citric acid cycle is a target for regulation in both prokaryotes and eukaryotes. In bacteria, IDH is regulated by phosphorylation by IDH kinase/phosphatase, wheras in animals, IDH is subject to allosteric regulation. In bacteria, IDH is inactivated by phosphorylation during growth on acetate in order to shunt acetyl groups to the glyoxalate bypass (Fig. 1), which generates new biosynthetic precursors. The work described in this thesis was intended to elucidate the regulatory and catalytic mechanisms of the NADP$^+$-dependent IDH of *Escherichia coli.*

Protein phosphorylation, in which a kinase transfers the γ-phosphate of ATP to an amino acid residue of a protein, has proved to be a ubiquitous mechanism for regulation of cellular proteins. Protein phosphorylation is most commonly at serine, threonine, or tyrosine side chains, and is normally reversible, with the protein phosphate hydrolyzed to inorganic phosphate by a phosphoprotein phosphatase. Because post-translational modifications of proteins such as phosphorylation may be carried out much faster and with far less energetic cost than synthesis or degradation of proteins, they provide an efficient means for the rapid response of a cell to changing conditions. Reversible phosphorylation cycles are also capable of greatly enhancing both the magnitude and sensitivity of the cellular response to changing conditions. Protein phosphorylation is thus involved not only in post-translational regulation, but mediates regulation at the transcriptional and translational levels as well. Regulatory protein phosphorylation was first characterized in glycogen phosphorylase, and today literally dozens of new cases are reported annually. It has been estimated that from one out of ten to one out of six proteins are subject to control by reversible phosphorylation. Examples of protein phosphorylation can be found not only in the metabolism of carbohydrates, lipids, and amino acids, but in ion channels of the nervous system, neurotransmitter biosynthesis, polyamine biosynthesis, photosynthesis, and transcriptional and translational control, to name just a few. Perhaps most intriguing are the recent findings that many oncogene products and growth factor receptors are tyrosine kinases, and that protein phosphorylation plays a key role in control of the cell cycle.

The *icd* gene of *Escherichia coli* encoding IDH has been sequenced, and appears to be homologous only with isopropylmalate dehydrogenase, a metal-dependent enzyme involved in leucine biosynthesis catalyzing essentially the same reaction as IDH on a different substrate. Many other nucleotide binding proteins, most notably the NAD^+-dependent dehydrogenases, have nucleotide-binding domains with very similar folding topologies. In the most similar cases, such as the lactate dehydrogenase-like family of NAD^+-dependent dehydrogenases, a common evolutionary history could be inferred from the topological similarity of the structures. It was therefore of interest to determine whether IDH possessed such a fold, as this might indicate a common evolutionary origin obscured by drift in the one-dimensional nucleotide sequence.

To understand the mechanisms of regulation and catalysis, and to determine the possible evolutionary relationship to other dehydrogenases, three-dimensional structures of IDH in dephosphorylated, phosphorylated, and substrate-bound forms were required. The only practical approach to obtain detailed information on the structure of a IDH, a dimer of identical 416-residue subunits, was x-ray crystallography. X-ray crystallography was first developed by Laue and Bragg, and first applied to proteins by Bernal and Perutz. Because IDH showed no great sequence similarity to any protein of known structure, the only available method was isomorphous replacement. Several recent advances to crystallographic methodology proved very useful in the structure determination of IDH: multiwire proportional counters for intensity measurement, solvent flattening, and simulated annealing.

The structure of dephosphorylated IDH was initially determined in the absence of ligands, and is described in chapter 2. In order to understand the effect of phosphorylation, the structure of the phosphorylated enzyme was solved, as described in chapter 3. A complete understanding of regulation and catalysis required knowledge of the interactions of substrate and enzyme, and the structure of IDH with Mg^{++} and isocitrate bound was solved for this reason. The implications of this structure for regulation are described in chapter 4, and the catalytic mechanism is discussed in chapter 5.

Figure 1

The citric acid cycle and the glyoxalate bypass, showing the branchpoint at isocitrate (after C. S. Stueland, K. Gorden, and D. C. LaPorte (1988) *J. Biol. Chem.* **263**:19475-19479).

Figure 2

Structural formula for the two-step reaction catalyzed by IDH.

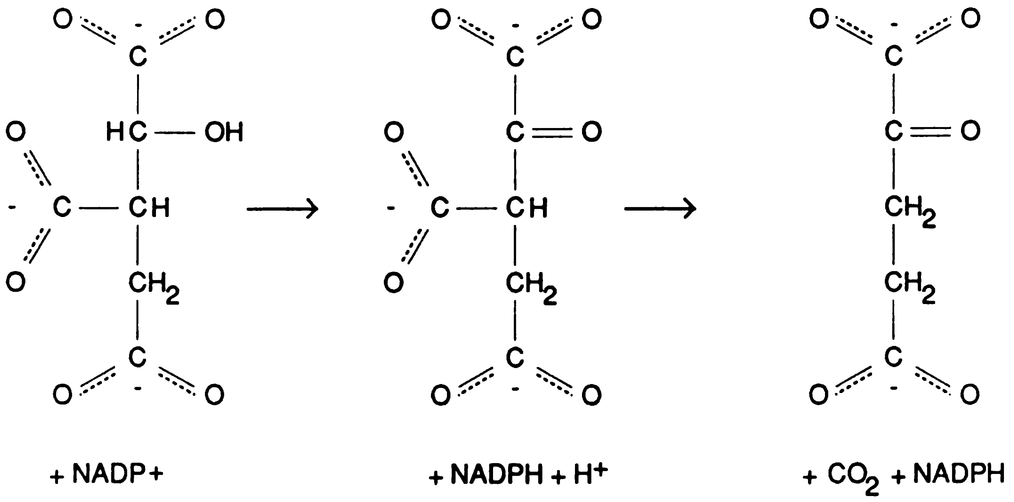
+ NADP+
+ NADPH + H+
+ CO2 + NADPH

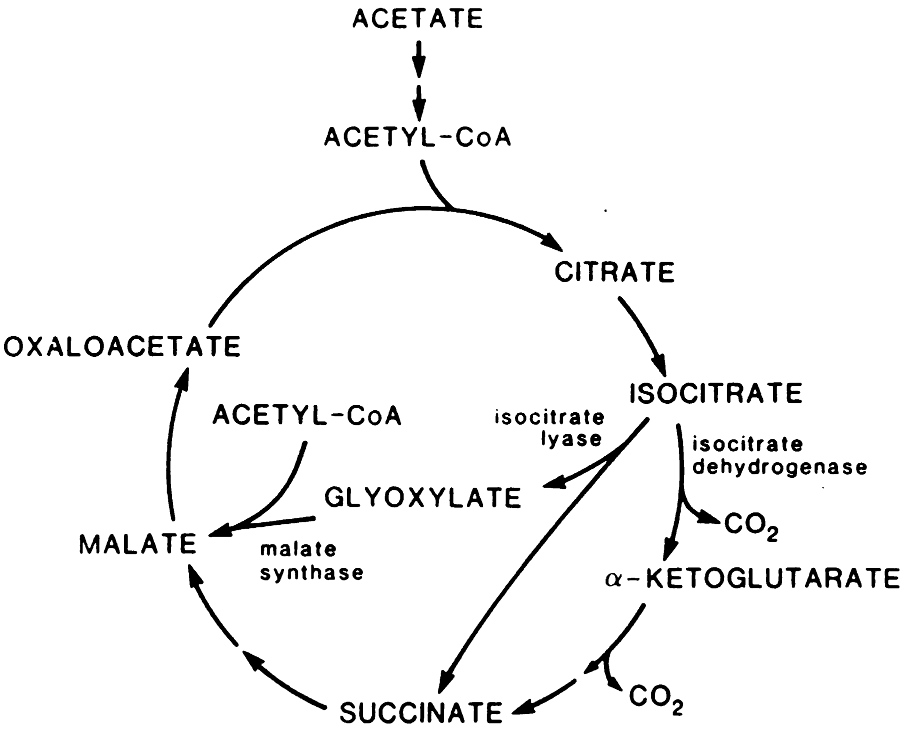
ACETATE
ACETYL-CoA
CITRATE
OXALOACETATE
ISOCITRATE
ACETYL-CoA
isocitrate lyase
isocitrate dehydrogenase
GLYOXYLATE
CO_2
MALATE
malate synthase
α-KETOGLUTARATE
SUCCINATE
CO_2

STRUCTURE OF A BACTERIAL ENZYME REGULATED BY PHOSPHORYLATION, ISOCITRATE DEHYDROGENASE

James H. Hurley[*], Peter E. Thorsness[†,†] , V. Ramalingam[*], Nancy H. Helmers[*],
Daniel E. Koshland, Jr.[†] and Robert M. Stroud[*,§]

[*]Department of Biochemistry and Biophysics and Graduate Group in Biophysics
University of California
San Francisco, Ca. 94143-0448

[†]Department of Biochemistry
University of California
Berkeley, Ca. 94720

§. To whom correspondence should be addressed.

†. Current address is Section of Genetics and Development, Cornell University, Ithaca, N.Y. 14853

Abbreviations: IDH, isocitrate dehydrogenase; IMDH, isopropylmalate dehydrogenase; LDH, lactate dehydrogenase.

The structure of isocitrate dehydrogenase from *Escherichia coli* has been solved and refined at 2.5 angstroms resolution, and is topologically different from that of any other dehydrogenase. This enzyme, a dimer of identical 416-residue subunits, is inactivated by phosphorylation at Ser 113, which lies at the edge of an interdomain pocket that also contains many residues conserved between isocitrate dehydrogenase and isopropylmalate dehydrogenase. Isocitrate dehydrogenase contains an unusual clasp-like domain in which both polypeptide chains in the dimer interlock. Based on the structure of isocitrate dehydrogenase and conservation with isopropylmalate dehydrogenase, we suggest that the active site lies in an interdomain pocket, close to the phosphorylation site.

The isocitrate dehydrogenase (IDH) of *Escherichia coli* (threo-Ds-isocitrate:NAD(P)$^+$ oxidoreductase [decarboxylating]; E.C. 1.1.1.42) is subject to a unique mechanism of regulatory control. This enzyme lies at a key branch point in carbohydrate metabolism which is extremely sensitive to regulation (1-5); it is converted from an active to a completely inactive form upon phosphorylation (1).

The reaction catalyzed by IDH is a step in the citric acid cycle, and is shown in equation 1.

1. $\mathrm{NAD(P)^+} + \text{isocitrate} \dashrightarrow \mathrm{NAD(P)H} + \alpha\text{-ketoglutarate} + \mathrm{CO_2}$

The enzyme was shown to be phosphorylated (6,7) and that the phosphorylation occured on a serine residue (8). Although there is some loss of activity when Ser 113 is replaced by a number of amino acids (Ala, Cys, Thr, Tyr), the replacement by aspartic acid causes complete inactivation (9). Hence, it is the negative charge introduced by phosphorylation that causes inactivation (9).

There is no significant sequence conservation between IDH and any of the dehydrogenases for which three-dimensional structures are known. The sequence of *E. coli* IDH shows significant conservation only with isopropylmalate dehydrogenase (IMDH) (9). A preliminary x-ray diffraction pattern has been reported for IMDH (10). Aligned residues of IDH and IMDH sequences (11-14) are 25 % to 29 % identical, varying among species.

The structures of dehydrogenases have been the subject of much interest because the nucleotide-binding domains of many of these enzymes retain much structural similarity, despite relatively little sequence conservation, as first observed by Rossmann, et. al. (15). This nucleotide-binding fold is referred to as the lactate dehydrogenase (LDH) fold, for the first enzyme in which it was described (16). The same fold has been described, with small modifications, in many other structures, frequently in a nucleotide-binding domain. As IDH shows no sequence conservation with dehydrogenases of known structure, the IDH structure is of interest as a potential alternative solution to the same evolutionary challenge.

Structure Determination

IDH was purified by a modification of the procedure described by Reeves et. al. (17) from a strain of *E. coli* in which IDH was expressed as described by LaPorte et. al. (18). Crystals were grown in a solution containing 28 mg/ml dephosphorylated IDH, 34 % saturated ammonium sulfate, 100 mM NaCl, 35 mM Na_2HPO_4, 9 mM citric acid and 0.2 mM DTT at pH 5.4 . Crystals grew to a size of 0.8 mm along the largest dimension after two weeks. Unit cell parameters are a = b = 105.1 Å, c = 150.3 Å and the space group is $P4_32_12$. The asymmetric unit is the monomer; two monomers are related by crystallographic two-fold symmetry.

Diffraction was observed to 2.5 Å with Cu Kα radiation from a rotating anode x-ray source at room temperature. All diffraction data were collected on a Nicolet area detector and reduced with the XENGEN data reduction package. One isomorphous heavy atom derivative was prepared by a five-day soak in 1% saturated p-chloromercuribenzenesulfonic acid (PCMBS). The position of one major site was determined from the heavy-atom difference Patterson map, with a second site subsequently located from an error residual map. Heavy atom parameters were refined by the method of Dickerson (19) and a single isomorphous replacement (SIR) electron density map was calculated. Crystallographic statistics as a function of resolution are summarized in figure 1.

Density modification (20), resulted in a dramatic improvement of the electron density map. The unusually large solvent fraction of 0.73 facilitated the use of density modification in phasing. The phases calculated by a first round of density modification were fixed and used for further refinement of heavy atom parameters; a second SIR map was used in new round of density modification, and a second density-modified phase set was calculated. 10 cycles of density modification resulted in a final R-factor of 28 % and a mean figure of merit of 0.76.

The main chain was built into a 2.8 Å electron-density map as polyalanine with FRODO (21). Phase combination between a 375-residue partial structure and SIR phases allowed us to fit amino acid sequence to the electron density for the entire model. PCMBS sites are at Cys 332 and Cys 405. Refinement then proceeded with alternate cycles of minimization using PROLSQ (22) and XPLOR (23) and manual rebuilding with the aid of

$(2F_o-F_c)\alpha_{calc}$ Fourier syntheses. The placement of some 40 residues changed substantially during refinement; 7 residues were added in the N-terminal region. $(2F_o-F_c)\alpha_{calc}$ maps based on phases calculated after refinement with PROLSQ after removal of residues in question were used to test the model; these led to no reconnections. The current model has been refined by simulated annealing using XPLOR for 1 ps at 2000° K and 0.25 ps at 300° K, followed by minimization and manual rebuilding into a 2.5 Å map. The first four residues from the N-terminus have not been placed in electron density in the current model. The fit of side chains to electron density (Fig. 2) is generally excellent, and carbonyl oxygens can be seen in almost all of the map. The crystallographic R-factor is currently 19.7% for 17948 reflections with $|F|/\sigma(F) > 3$ from 5.0 to 2.5 Å (Fig. 1). The r.m.s. deviations of bond lengths and angles from ideal values are 0.017 Å and 3.4°, respectively.

The Structure of IDH

Domain structure. IDH consists of three domains: a large $\alpha+\beta$ domain, a small α/β domain, and an α/β clasp-like domain involving both subunits (Fig.s 3,4). The large and small domains are built around a common 12-stranded β sheet. A very distinct cleft separates the large and small domains, and except for the sheet they are folded independently, each with its own hydrophobic core. Two pockets line the cleft between the large and small domains, one on either side of the sheet. We will refer to the pockets formed in front of and behind the sheet, as viewed in figure 3, as the "front" and "rear" pockets. The exceptionally large β sheet is mixed parallel and antiparallel and comprises 270° of a turn of superhelix, which has the normal left-handed sense. 99% of the expected sequence has been located; IDH is 46 % helical, 22 % sheet, 19 % coil and 12% turn.

The small domain consists of residues 125-157 and 203-317, and is a typical α/β sandwich structure. The large domain consists of residues 1-124 and 318-416. This domain has a helical subdomain consisting of helices a, j, k, l, and m, and a large α/β subdomain, which makes up the rest of the large domain. Helices a and j are packed against the sheet, hence belonging to both the helical bundle and the α/β subdomains.

The clasp-like domain is formed by the interlocking about the crystallographic two-fold axis of the polypeptide segments consisting of residues 158 through 202 from both subunits (Fig. 5). A flat four-stranded antiparallel β sheet is formed by two strands from each subunit. A hydrophobic core is formed only in the dimer by the packing of the helices against each other and the sheet. The small domain as well as the clasp-like domain are involved in inter-subunit contacts. Helices h and i form extensive hydrophobic contacts with helices i' and h' (where the ' denotes the other subunit). Residues 140 and 234-236, which are in loops and at the start of the g helix, are also involved in intersubunit contacts.

Phosphorylation site. The phosphorylation site at Ser 113 is on helix d, at the edge of the front pocket (Fig. 6). Most of the regions of highest conservation between IDH and IMDH sequences (Fig. 7) are in the cleft. Strands D, F and G, part of the floor of both pockets, are all at least 50% conserved. Also highly conserved are helix i and loops 230-234 and 339-347 in the front pocket region, and helix j. Strand N (Fig. 7) is not present in

IMDH, and strand M is not conserved. Three conserved arginines, Arg 119, 129 and 153, near Ser 113, and His 339, the only conserved histidine, are in the front pocket. Lys 230', another conserved residue, also points into this pocket. The rear pocket is highly hydrophobic, and includes residues Tyr 125, Leu 128, Ile 328, Phe 335 and Met 362, similar or identical in IMDH.

Discussion

Topology. The topology of IDH (Fig. 8) is quite distinct from that described for the known dehydrogenase structures. Best known is the lactate dehydrogenase-like class, including lactate dehydrogenase (LDH) (16), malate dehydrogenase (25), alcohol dehydrogenase (26), glyceraldehyde 3-phosphate dehydrogenase (27), and L-3-hydroxyacyl CoA dehydrogenase (28). Although the catalytic domains vary in structure, the nucleotide-binding domains of these enzymes all have a very similar structure, the LDH fold, and all bind the cofactor in a similar manner. The LDH fold consists of a $\beta\alpha\beta\alpha\beta$ motif, with the β strands arranged in parallel and linked by parallel helices. In the LDH-like dehydrogenases, the motif is repeated twice, and is also referred to as a "dinucleotide-binding fold"; a single $\beta\alpha\beta\alpha\beta$ unit is also referred to as a "mononucleotide-binding fold". Minor variations, such as the absence of a single helix, occur within this family. Many other proteins, either nucleotide-binding or with other functions, are topologically similar to the LDH-like class; an extensive review of α/β topologies is given by Richardson (29). Only NAD(P)$^+$-binding proteins are discussed here.

A second group of dehydrogenases has structural similarity to glutathione reductase (30), and includes trimethylamine dehydrogenase (31) and lipoamide dehydrogenase (32). These enzymes have only an LDH-like mononucleotide-binding fold, within a larger parallel sheet. Still less similar to LDH, dihydrofolate reductase (33) contains an LDH-like mononucleotide-binding fold within a mixed parallel and antiparallel sheet.

Nearly all known α/β nucleotide binding domains exploit the partial positive charges at the N-termini of parallel α helices in binding the negatively charged phosphate moities of the nucleotide (34). Among the dehydrogenases, so far only 6-phosphogluconate dehydrogenase (35), an α helical protein, is outside the α/β class. Beef liver catalase binds NADPH near the C-terminus of a helix (36), although the function of NADPH in this system is unknown. The IDH structure contains four α helices in a parallel arrangement packed on either side of a section of parallel β sheet, in a manner typical of nucleotide binding domains. Although the location of bound $NADP^+$ has yet to be determined, it is possible that the IDH fold has evolved to provide the same electrostatic enhancement of nucleotide binding by terminal partial charges of parallel helices enjoyed by the LDH-like enzyme class.

Although the topology of IDH is quite distinct from that of LDH, part of the small domain of IDH consists of parallel helices packed on either side of a parallel section of β sheet, resembling the LDH-like mononucleotide binding domain. This feature contains the four parallel strands G-J and helices f-i. If the clasp-like domain and strands K and L were removed, the arrangement in the sheet of strands G-J numbered as they occur in the sequence would be 1, 4, 2, 3. If the connections to strands G and H were exchanged, the arrangement in the sheet would then be 4, 1, 2, 3. Helices f and g would then connect strands 1, 2, 3, forming an LDH-like mononucleotide-binding fold. Careful inspection of an electron density map calculated with phases from a model refined after omitting strands G and H assures us, however, that these connections cannot be exchanged.

To compare the IDH and LDH structures in three dimensions, helices f and g and strands G-J of IDH, and helices B and C and strands D, A, B and C of LDH* were superposed by least-squares. The r.m.s. deviation between the main chain atoms of these 50 residues is only 2.8 Å. The rest of the 152 residues in the small domain of IDH do not superpose well with the LDH nucleotide-binding domain. Only a few types of supersecondary structure are common in proteins, and secondary structural elements in α/β stuctures tend to pack at the same angles in diverse proteins (37). Topologies of IDH and LDH are dissimilar, and evolutionary relatedness cannot be inferred solely from similar supersecondary structure.

IDH contains a fold which has not previously been described. Within the spectrum of topologies of α/β structures in NAD(P)$^+$-binding proteins, the small domain of IDH is among the most different from the LDH fold. We expect the overall structure of IMDH to be similar, although probably lacking a separate clasp-like domain and without the N-terminal loop of IDH. It is likely that the evolutionary histories of IDH and related enzymes are different from those of most other dehydrogenases.

Clasp-like domain. The unusual interlocking clasp-like domain is based on a β sheet in which both identical polypeptide chains from the dimer contribute strands. The 60° packing angle of helices with the sheet, and the hydrogen-bonding of symmetry-related strands make this domain similar to that formed jointly by the α1 and α2 domains in the class I human leukocyte antigen (HLA) (38). Among other examples, the subunit interface in alcohol dehydrogenase (27) contains two sets of symmetry-related antiparallel β strands.

Conservation, binding, catalysis and regulation. The phosphorylation site at Ser 113 (Fig. 6) is sufficiently close to the subunit interface to allow direct interactions between the phosphoserine and the other subunit. In contrast to the case of glycogen phosphorylase, in which the region of the phosphorylation site is well ordered only in the phosphoenzyme (39), Ser 113 and surrounding residues of dephosphorylated IDH are well ordered. Ser 113 is on the protein surface, presumably accessible to IDH kinase/phosphatase. Ser 113 is also at the edge of the front pocket, compatible with a possible direct phosphoserine-substrate interaction. There is a cluster of conserved residues in the pocket, including Arg 119 , Arg 129, Arg 153, Tyr 160, and Lys 230'. The conserved positive charges suggest a binding site for negatively charged substrates, and perhaps a means for stabilizing the oxyanion intermediate that is believed to occur in the IDH reaction. Lys 230' is in the loop 230-234 adjoining the pocket, suggesting that both subunits participate in each active site. The only conserved histidine, His 339, is also in this pocket, in the highly conserved loop 339-347, and is a candidate for the acid-base catalyst normally present in dehydrogenases. The exceptional hydrophobicity and the high level of conservation in the rear pocket suggest some functional importance for this pocket as well.

As demonstrated in glycogen phosphorylase, regulatory covalent modifications and allosteric control can cause conformational changes that propagate over large distances (39). Covalent phosphorylation of IDH is particularly dramatic because the negative charge on the phosphoserine reduces activity to essentially zero. Whether the regulatory effect is through a confomational change, a direct charge effect on one or more of the substrates or a combination of the two awaits the structural analysis of the phosphoenzyme and complexes with substrate and cofactor.

Acknowledgments

We thank Janet Finer-Moore and William Montfort and for valuable comments on the structural analysis, J. Fernando Bazan for suggestions concerning sequence comparisons and Tony Dean for helpful discussions. Eric Fauman assisted in preliminary characterization of IDH crystals, and Julie Newdoll helped prepare figures 3 and 5. This work was supported by grants GM 24485 to R.M.S. and NSF 04200 to D.E.K. Crystallographic refinement was carried out in part on Pittsburgh Supercomputer Center facilities under grant DMB890040P. J. H. thanks the UC Regents for a fellowship. Atomic coordinates have been deposited at the Brookhaven Protein Data Bank.

References

1. LaPorte, D.C. and Koshland, D.E., Jr. (1983) *Nature* **305**, 286-290.

2. Kornberg, H.L. and Madsen, N.B. (1951) *Biochim. Biophys. Acta* **24**, 651-653.

3. Kornberg, H.L. (1966) *Biochem. J.* **99**, 1-11.

4. Holms, W.H. and Bennett, P.M. (1971) *J. Gen. Microbiol.* **65**, 57-68.

5. LaPorte, D.C., Walsh, K. and Koshland, D.E., Jr. (1984) *J. Biol. Chem.* **259**, 14068- 14075.

6. Garnak, M. and Reeves, H.C. (1979) *J. Biol. Chem.* **254**, 7915-7920.

7. Wang, J.Y.J. and Koshland, D.E., Jr. (1982) *Arch. Biochem. Biophys.* **218**, 59-67.

8. Borthwick, A.C., Holms, W.H. and Nimmo, H.G. (1984) *Biochem. J.* **222**, 797-804.

9. Thorsness, P.E. and Koshland, D.E., Jr. (1987) *J. Biol. Chem.* **262**, 10422-10425.

10. Katsube, Y., Tanaka, N., Takenaka, A., Yamada, T., and Oshima, T. (1988) *J. Biochem*, **104**, 679-680.

11. Kagawa, Y., Nojima, H., Nukiwa, N., Ishizuka, M., Nakajima, T., Yasuhara, T., Tanaka, T. and Oshima, T. (1984) *J. Biol. Chem.* **259**, 2956-2960.

12. Imai, R., Sekiguchi, T., Nosoh, Y. and Tsuda, K. (1987) *Nucl. Acid Res.* **15**, 4988.

13. Sekiguchi, T., Suda, M., Ishii, T., Nosoh, Y. and Tsuda, K. (1987) *Nucl. Acid Res.* **15**, 853.

14. Hamasawa, K., Kobayashi, Y., Harada, S., Yoda, K., Yamasaki, M. and Tamura, G. (1987) *J. Gen. Microbiol.* **133**, 1089-1097.

15. Rossmann, M.G., Moras, D. and Olsen, K.W. (1974) *Nature* **250**, 194-199.

16. Adams, M.J., Ford, G.C., Koekok, R., Lentz, P.J.,Jr., McPherson, A., Jr., Rossmann, M.G., Smiley, I.E., Schevitz, R.W. and Wonacott, A.J. (1970) *Nature* **227**,1098- 1103.

17. Reeves, H.C., Gaston, O.D., Chen, C.L. and Houston, M. (1972) *Biochim. Biophys. Acta* **258**, 27-39.

18. LaPorte, D.C., Thorsness, P.E. and Koshland, D.E. Jr. (1985) *J. Biol. Chem.* **260**, 10563-10568.

19. Dickerson, R.E., Weinzierl, J.E. and Palmer, R.A. (1968) *Acta Cryst.* **B24**, 997- 1003.

20. Wang, B.C. (1985) ***Methods** Enzymol.* **115,** 90-111.

21. Jones, T.A. (1985) ***Methods** Enzymol.* **115,** 157-170.

22. Hendrickson, W.A. (1985) ***Methods** Enzymol.* **115**, 252-270.

23. Brunger, A.T., Kuriyan, K. and Karplus, M. (1987) *Science* **235**, 458-460.

24. Devereux, J., Haeberli, P. and Smithies, O. (1984) *Nucl. Acids Res.* **12**(1), 387-395.

25. Hill E. , Tsernoglou, D., Webb, L.and Banaszak, L.J. (1972) *J. Mol. Biol.* **72**, 577- 591.

26. Branden, C.I., Eklund, H., Nordstrom, B., Boiwe, T., Soderlund, G., Zeppezauer, E., Ohlsson, I. and Akeson, A. (1973) *Proc. Natl. Acad. Sci. USA* **70**, 2439-2442.

27. Buehner, M., Ford, G.C., Moras, D., Olsen, K.W., and Rossmann, M.G. (1973) *Proc. Natl. Acad. Sci. USA* **70**, 3052-3054.

28. Birktoft, J.J., Holden, H.M., Hamlin, R., Xuong, N.H. and Banaszak, L.J. (1987) *Proc. Natl. Acad. Sci. USA* **84**, 8262-8266.

29. Richardson, J.S. (1981) *Adv. Protein Chem.* **34**, 167-339.

30. Thieme, R., Pai, E.F., Schirmer, R.H. and Schulz, G.E. (1981)*J. Mol. Biol.* **152**, 763- 782.

31. Lim, L.W., Shamala, N., Mathews, F.S., Steenkamp, D.J., Hamlin, R. and Xuong, N. (1986) *J. Biol. Chem.* **261**(32),15140-15146.

32. Takenaka, A., Kizawa, K., Hata, T., Sato, S., Misaka, E., Tamura, C. and Sasada, Y. (1988) *J. Biochem* **103**, 463-469.

33. Wierenga, R.K., De Maeyer, M. C. H. and Hol, W. G. J. (1985) *Biochemistry* **24**, 1346-1357

34. Adams, M.J., Archibald, I.G., Bugg, C.E., Carne, A., Gover, S., Helliwell, J.R., Pickersgill, R.W. and White, S.W. (1983) *EMBO J.* **2**, 1009-1014.

35. Matthews, D.A., Alden, R.A., Bolin, J.T., Filman, D.J., Freer, S.T., Hamlin, R., Hol, W.G.J., Kisliuk, R.L., Pastore, E.J., Plante, L.T., Xuong, N. and Kraut, J. (1978) *J. Biol. Chem.* **253**, 6946-6954.

36. Fita, I. and Rossmann, M.G. (1985) *Proc. Natl. Acad. Sci. USA* **82**, 1604-1608.

37. Chothia, C. (1984) *Ann. Rev. Biochem.* **53**, 537-72.

38. Bjorkman, P.J., Saper, M.A., Samraoui, B., Bennett,W.S., Strominger,J.L. and Wiley, D.C. (1987) *Nature* **329**, 506-512.

39. Sprang, S.R., Fletterick, R.J., Goldsmith, E.J., Madsen, N.B., Acharaya, K.R., Stuart, D.J., Varvill, K. and Johnson, L.N. (1988) *Nature* **336**, 215-221.

Figure 1 Crystallographic statistics. $R_c = \Sigma|F_o-F_c|/\Sigma F_o$, summed over 17948 reflections with $|F|/\sigma(F) > 3$; F_o and F_c are the observed and calculated amplitudes. native Rmerge, PCMBS derivative Rmerge. $R_{merge} = \Sigma|I_i-\langle I\rangle|/\Sigma\langle I\rangle$, summed over all observations from all crystals. Of 30209 reflections possible from 25 to 2.5 Å, 27951 were measured for native, and of 21668 reflections possible from 25 to 2.8 Å, 20055 were measured for the PCMBS derivative. The average redundancy of measurement was 4.25 for the native data set, and 3.0 for the derivative; the overall unweighted merging R-factor on intensity was .12 for 5 native crystals and .14 for 3 derivative crystals. $\langle\Delta F\rangle/\langle F\rangle = \Sigma w|F_{ph}-F_p|/\Sigma w F_p$, where $w = 1/\sigma^2$, and σ is the estimated error. Weighting is used so that $\langle\Delta F\rangle/\langle F\rangle$ approximates the true difference in amplitudes, rather than the increase of R_{merge} with resolution. The mean unweighted absolute value of $\Delta F/F$ between native and derivative data sets is 0.21. $0.1^*\langle FH\rangle/\varepsilon$ is the mean absolute value of the PCMBS heavy atom structure factor divided by the estimated r.m.s. lack of closure error, based on centric reflections only. $R_{Cullis} = 0.58$ for the PCMBS derivative; $R_{Cullis} = \Sigma||F_{ph}\pm F_p|-F_h|/\Sigma|F_{ph}\pm F_p|$, where the summation is over all centric reflections. PCMBS statistics are shown for heavy atom parameters refined with phases calculated by a first round of density modification.

Figure 2 Electron density from a 2.8 Å $(2F_o-F_c)\alpha_{calc}$ map for residues 241-246. The three aromatic side chains in the sequence Phe-Lys-Asp-Trp-Gly-Tyr made this a distinctive marker for assignment of known sequence to the model. Lys and Asp side chains are not visible in this view.

Figure 3 Diagrammatic drawing of the IDH monomer. The large α+β domain containing the N and C termini is to the left, the small α/β domain to the right, and the clasp-like domain is pointing down. The domains are separated between strands E and F. Helices are labelled in alphabetical order as they occur in the chain, and strands are labelled as they occur in the two β sheets, from left to right in this view. Roman numerals I and II designate the front and rear pockets. The shaded rod represents the crystallographic two-fold axis of symmetry which relates the two subunits.

Figure 4 Carbon α trace of IDH. The phosphorylation site at Ser 113, the C-terminus at Met 416, the first well-ordered residue in the model, Val 5, and other residues of interest are labelled in this divergent stereo view.

Figure 5 Diagrammatic drawing of the clasp-like domain, shown looking down the crystallographic two-fold axis. One subunit is shaded.

Figure 6 Divergent stereo view of the front interdomain pocket of IDH. Side chains are shown for selected conserved residues and Ser 113. Both subunits are shown; Lys 230 belongs to the second subunit.

Figure 7 Alignment of amino acid sequences of *E. coli* IDH and *Bacillus subtilis* IMDH. Alignments of IDH to IMDH sequences from *Thermus aquaticus* (11), *B. subtilis* (12), *Bacillus caldotenax* (13), and *Candida utilis* (14) produced similar identities. Two other available sequences, from *Thermus thermophilus* and *Saccharomyces cerevissiae*, were not used, as they are very similar to the *T. aquaticus* and *C. utilis* sequences. Pairwise sequence alignments using a standard algorithm (24) of IDH and IMDH

sequences were modified by hand to eliminate gaps in conserved regions of secondary structure where possible. Residues which are identical in *E. coli* IDH and *B. subtilis* IMDH sequences are boxed. Secondary structures of IDH are shown above the corresponding sequence; β strands and α helices are designated by shaded and solid bars above the sequence, and labelled with upper and lower case letters, respectively. Numbering is for the IDH sequence; numbers are included for endpoints of regular secondary structures.

Figure 8 Schematic diagram of the IDH fold. A table of other protein topologies is found in reference 29.

Footnotes

* Main chain atoms of residues 208-221, 239-251, 149-154, 297-302, 223-228 and 275-279 of IDH, and residues 31-44, 53-65, 92-97, 23-28, 48-53 and 77-81 of pig heart LDH, were included in the superposition.

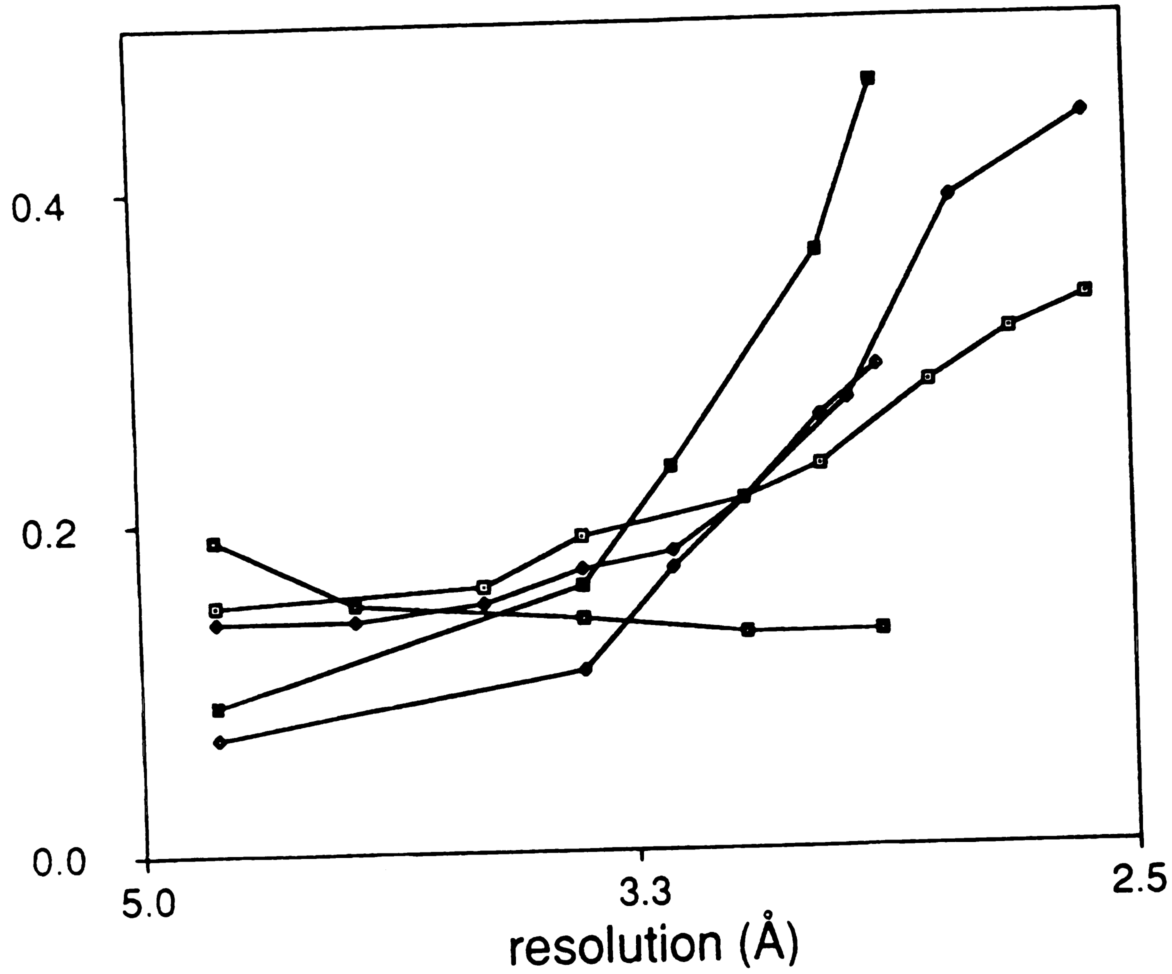
0.4
0.2
0.0
5.0
3.3
2.5
resolution (Å)

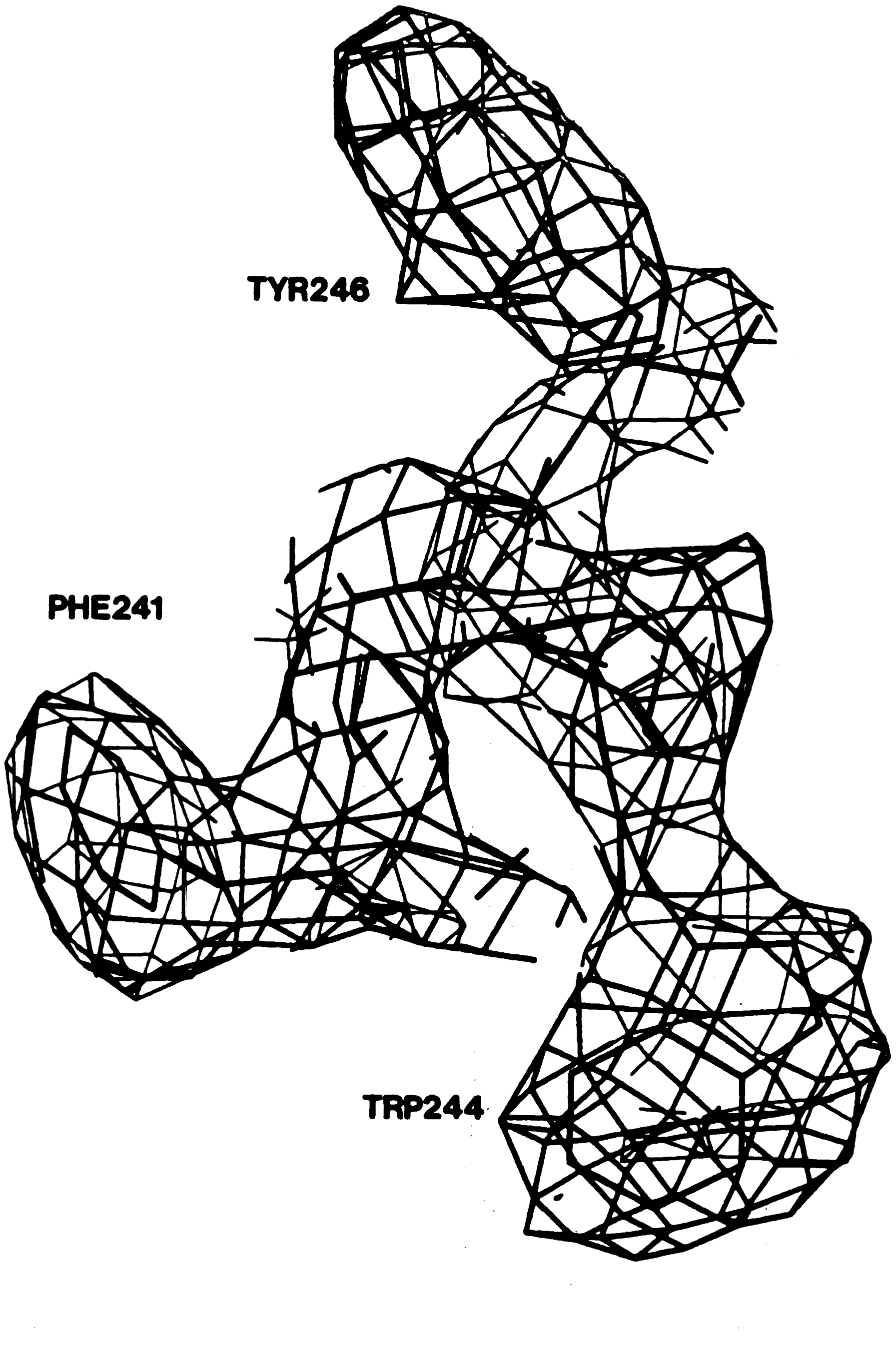

TYR246
PHE241
TRP244

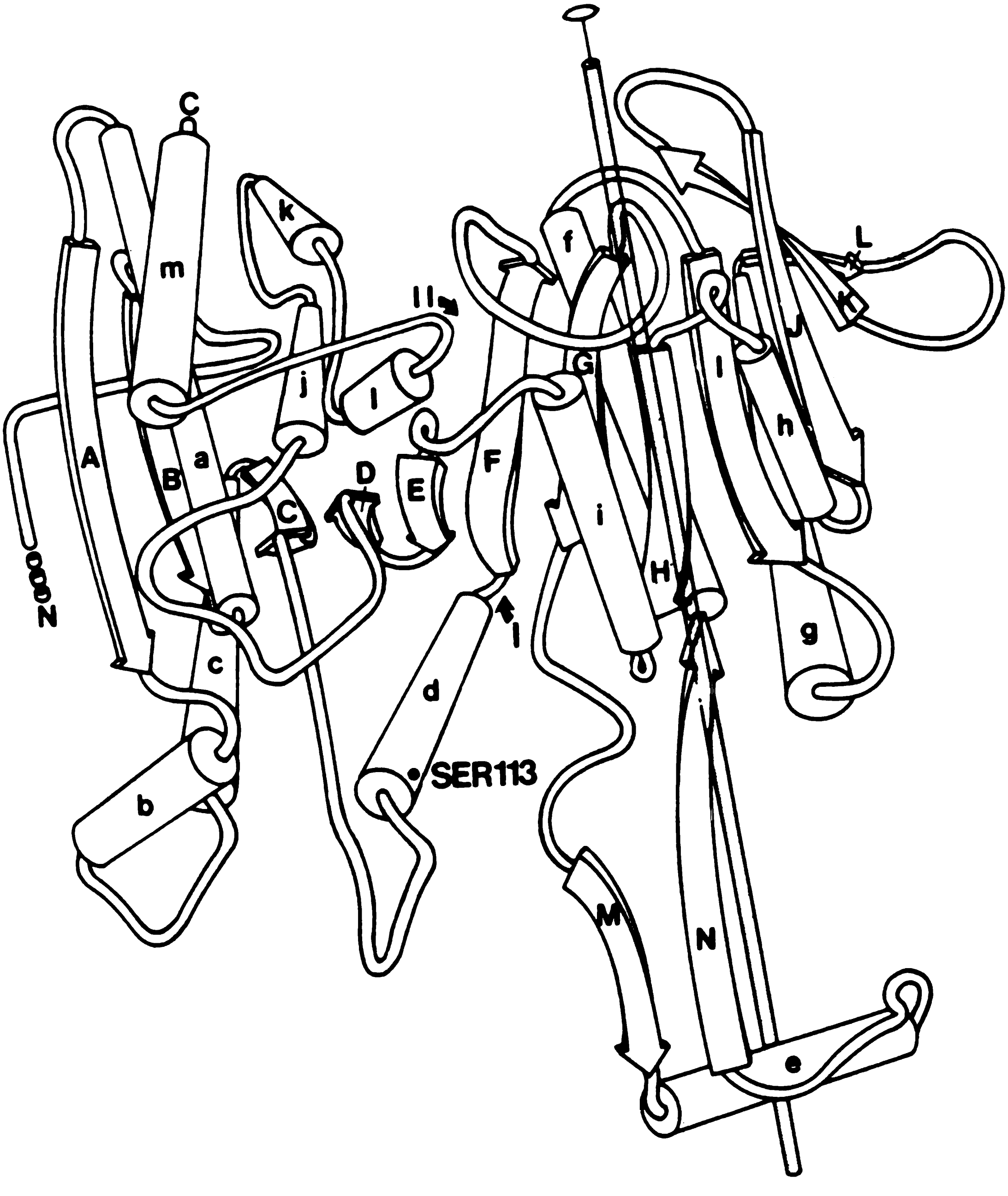
C
m
k
II
f
L
K
J
I
h
G
j
l
A
B
a
D
E
F
C
i
H
N
I
d
SER113
c
g
b
M
N
e

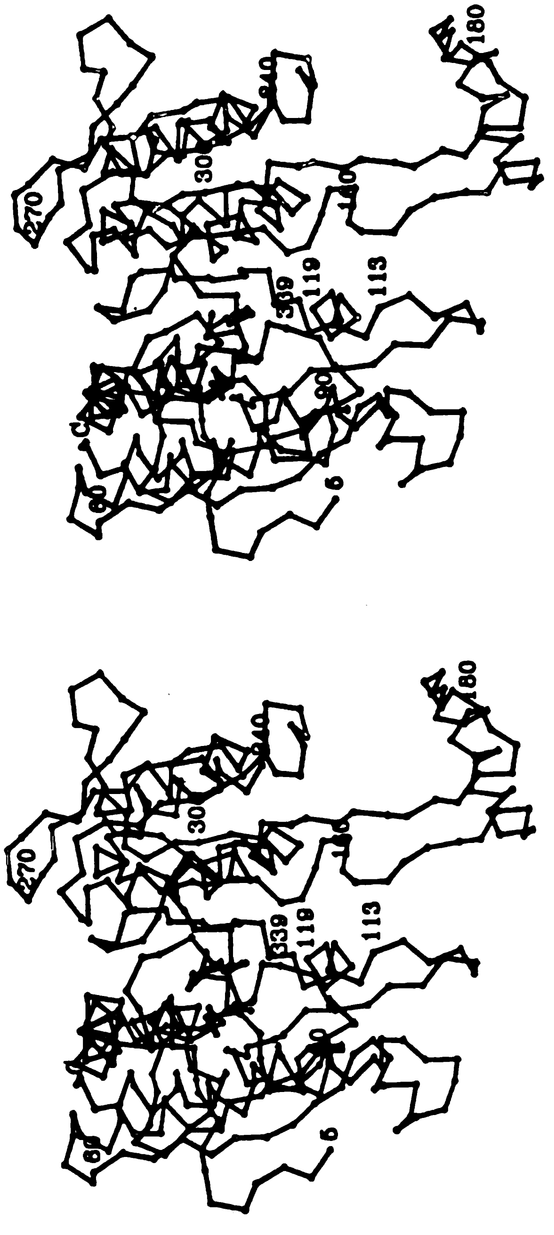
C

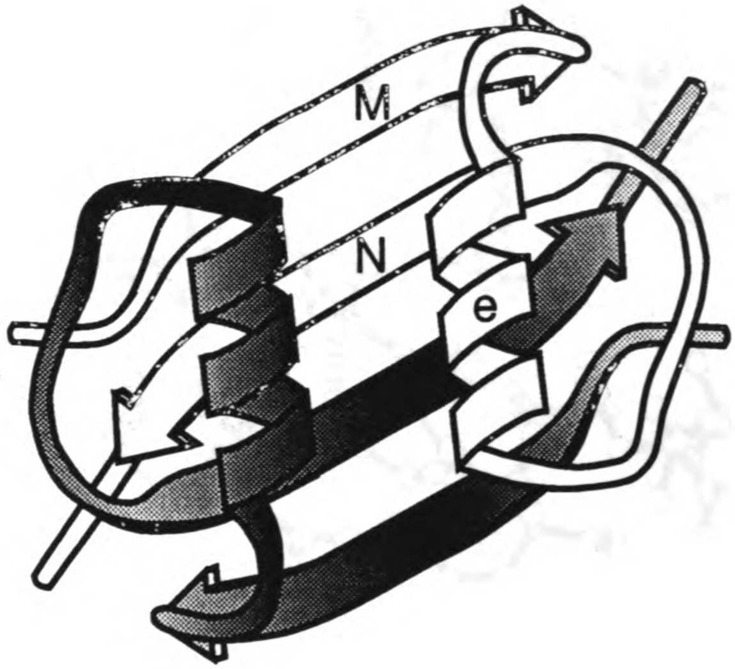
M
N
e

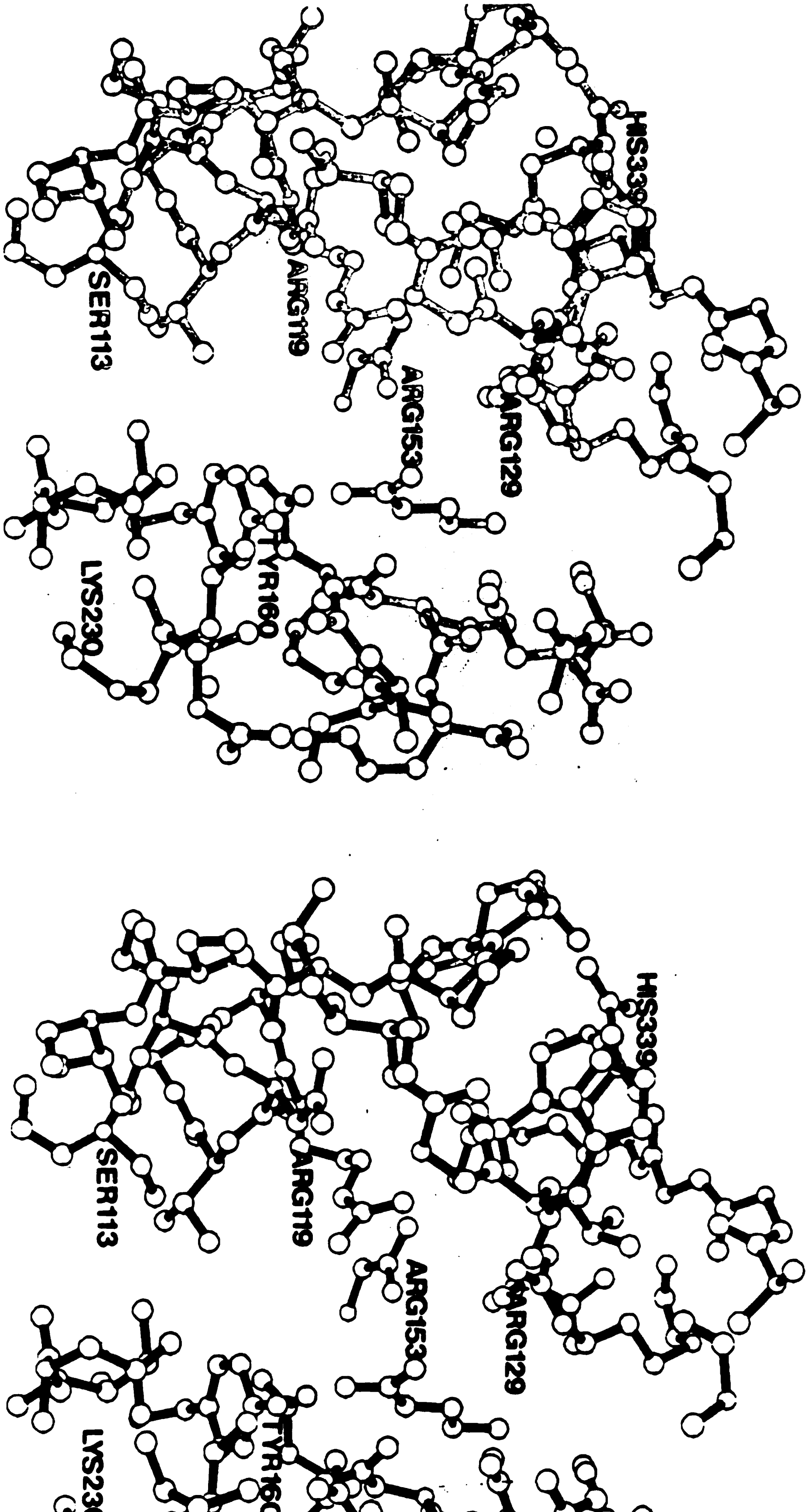
HIS339
SER113
ARG119
ARG153
ARG129
LYS230
TYR160

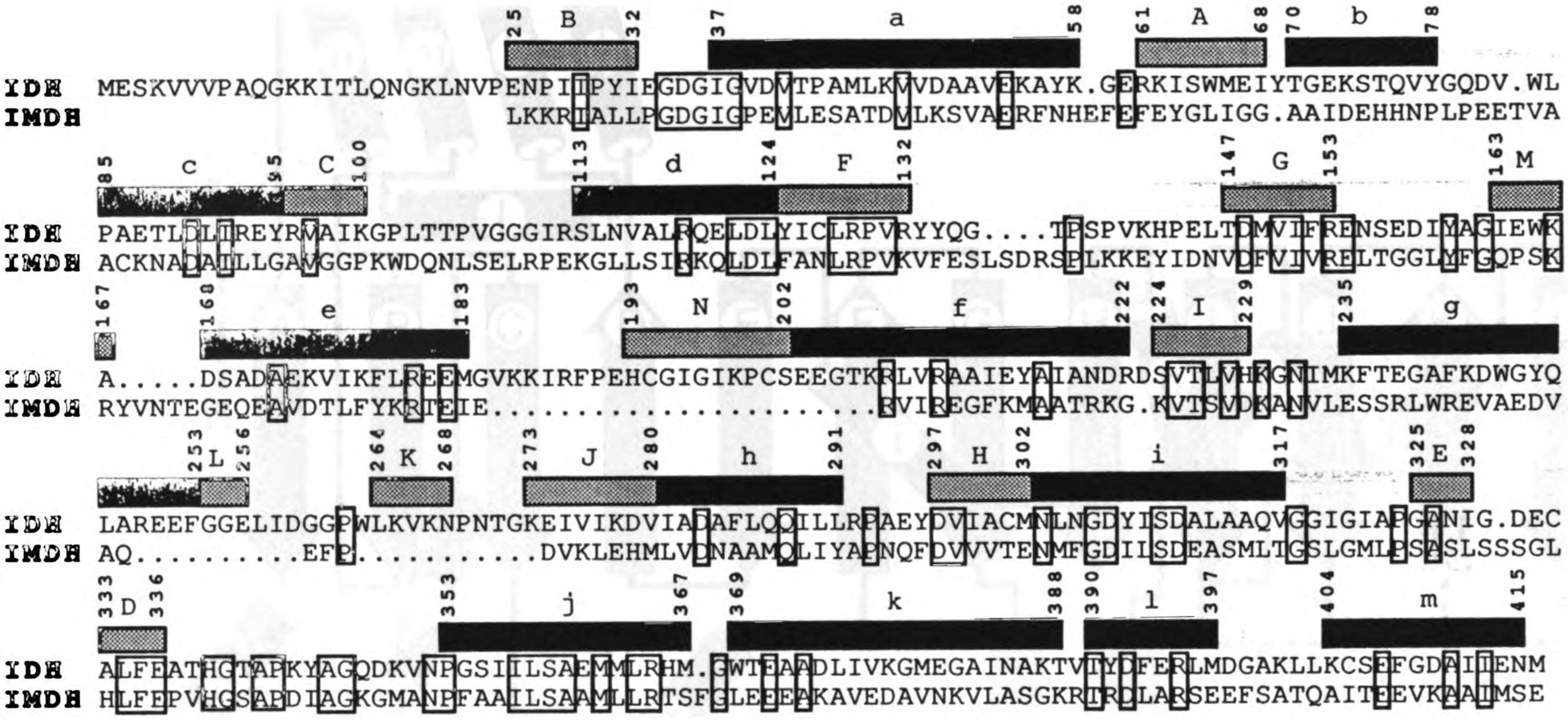
25 B 32
37 a 58
61 A 68
70 b 78
IDH MESKVVVPAQGKKITLQNGKLNVPENPIIPYIEGDGIGVDVTPAMLKVVDAAVEKAYK.GERKISWMEIYTGEKSTQVYGQDV.WL
IMDH LKKRIALLPGDGIGPEVLESATDVLKSVAERFNHEFEFEYGLIGG.AAIDEHHNPLPEETVA
85 c 95 C 100
113 d 124 F 132
147 G 153
163 M
IDH PAETLDLIREYRVAIKGPLTTPVGGGIRSLNVALRQELDLYICLRPVRYYQG....TPSPVKHPELTDMVIFRENSEDIYAGIEWK
IMDH ACKNADAILLGAVGGPKWDQNLSELRPEKGLLSIRKQLDLFANLRPVKVFESLSDRSPLKKEYIDNVDFVIVRELTGGLYFGQPSK
167
168 e 183
193 N 202 f 222
224 I 229
235 g
IDH A.....DSADAEKVIKFLREEMGVKKIRFPEHCGIGIKPCSEEGTKRLVRAAIEYAIANDRDSVTLVHKGNIMKFTEGAFKDWGYQ
IMDH RYVNTEGEQEAVDTLFYKRTEIE.....................RVIREGFKMAATRKG.KVTSVDKANVLESSRLWREVAEDV
253 L 256
264 K 268
273 J 280 h 291
297 H 302 i 317
325 E 328
IDH LAREEFGGELIDGGPWLKVKNPNTGKEIVIKDVIADAFLQQILLRPAEYDVIACMNLNGDYISDALAAQVGGIGIAPGANIG.DEC
IMDH AQ..........EFP...........DVKLEHMLVDNAAMQLIYAPNQFDVVVTENMFGDIILSDEASMLTGSLGMLPSASLSSSGL
333 D 336
353 j 367
369 k 388
390 l 397
404 m 415
IDH ALFEATHGTAPKYAGQDKVNPGSIILSAEMMLRHM.GWTEAADLIVKGMEGAINAKTVTYDFERLMDGAKLLKCSEFGDAIIENM
IMDH HLFEPVHGSAPDIAGKGMANPFAAILSAAMLLRTSFGLEEEAKAVEDAVNKVLASGKRTRDLARSEEFSATQAITEEVKAAIMSE

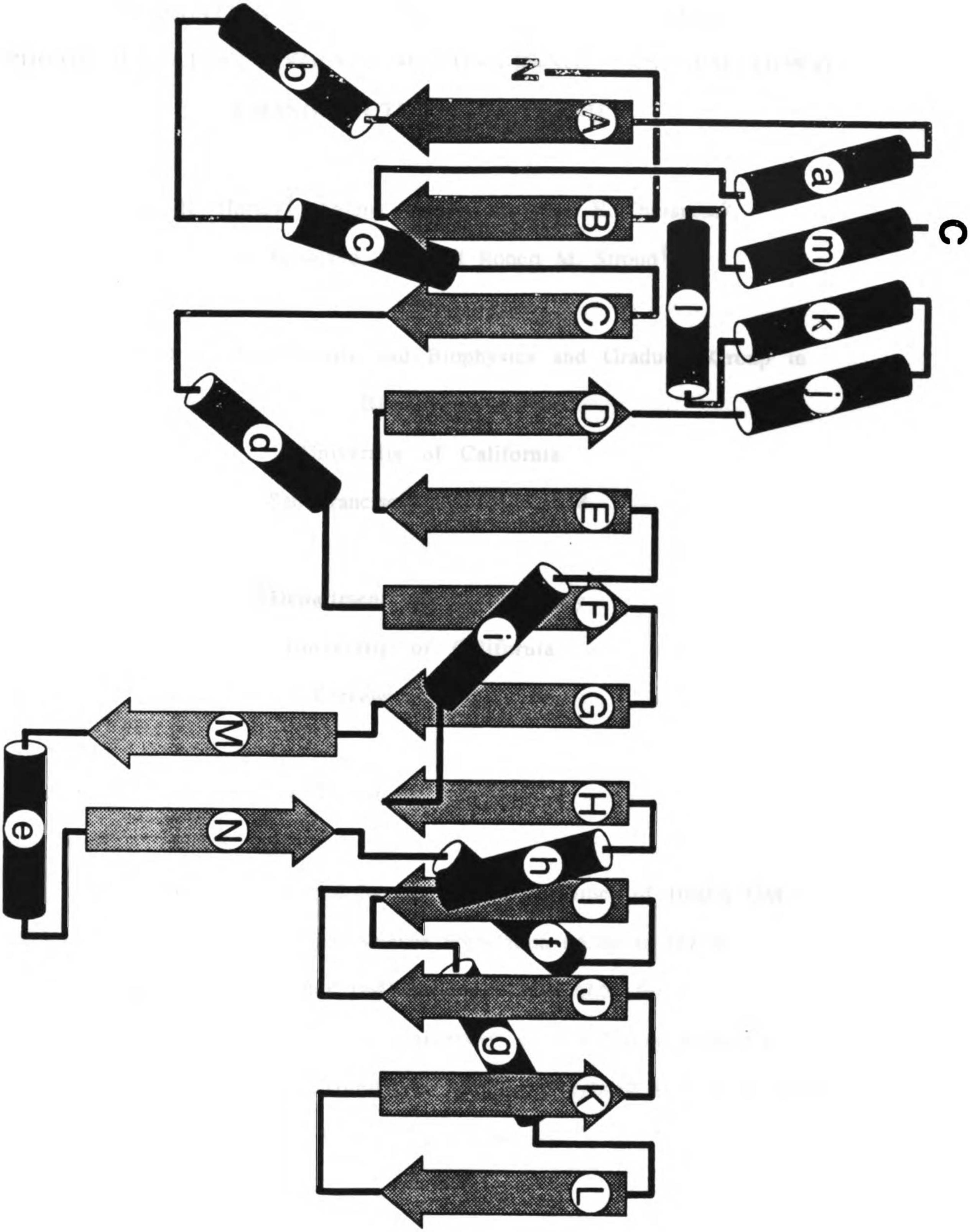
N
C
A
B
C
D
E
F
G
H
I
J
K
L
M
N
a
b
c
d
e
f
g
h
i
j
k
l
m

REGULATION OF ISOCITRATE DEHYDROGENASE BY PHOSPHORYLATION INVOLVES NO LONG-RANGE CONFORMATIONAL CHANGE IN THE FREE ENZYME

James H. Hurley[†], Antony M. Dean[§], Peter E. Thorsness[§],
Daniel E. Koshland, Jr.[§] and Robert M. Stroud[†,¶]

[†]Department of Biochemistry and Biophysics and Graduate Group in Biophysics
University of California
San Francisco, Ca. 94143-0448

[§]Department of Biochemistry
University of California
Berkeley, Ca. 94720

¶. To whom correspondence should be addressed.

This work was supported by the National Institues of Health GM 24485 to R.M.S. and the National Science Foundation 04200 to D.E.K., Pittsburgh Supercomputer Center DMB 890040P to R.M.S. for crystallographic refinement, and a University of California Regent's Fellowship to J.H.H. Atomic coordinates of phosphorylated IDH have been deposited at the Brookhaven Protein Data Bank.

The structure of the phosphorylated form of isocitrate dehydrogenase from *Escherichia coli* has been solved and refined to an R-factor of 16.9 % at 2.5 Å resolution. Comparison with the structure of the dephosphorylated enzyme shows that there are no large scale conformational changes, and that small conformational changes are highly localized around the site of phosphorylation at serine 113. Tyrosine 160 rotates by 15°, and there is a local rearrangement of water structure. There is an 0.2 Å net movement of loop 230-234, and side chain shifts of 0.2 Å r.m.s. for isoleucine 159 and lysine 199. The lack of large conformational changes, the observation of a possible isocitrate binding site close to serine 113 and the demonstration that the phosphorylated enzyme is unable to bind isocitrate, suggests that this enzyme is inactivated by a direct electrostatic interaction between the substrate and the serine phosphate.

Protein phosphorylation is a ubiquitous post-translation modification of central importance in the regulation of many cellular processes (1), with phosphorylation at serine most common (2). Protein phosphorylation has long been known to have a key role in the control of metabolism in eukaryotes (1,2), and in prokaryotes as well (3,4). Despite the importance of protein phosphorylation in many aspects of cellular biology, only the regulation of one enzyme, glycogen phosphorylase, has previously been described structurally (5). Recently, the structure of isocitrate dehydrogenase (*threo*-Ds-isocitrate:NAD(P)$^+$ oxidoreductase [decarboxylating]; E.C. 1.1.1.42) (IDH) from *Escherichia coli* , an enzyme regulated by phosphorylation (4,6), has been determined at 2.5 Å resolution (7). Phosphorylation of IDH, a functional dimer of 416-residue subunits, regulates the flux of substrate at a key branchpoint in carbohydrate metabolism (8,9,10,11) in response to changing nutritional conditions (8,9,12,13).

Phosphorylation occurs at serine 113 (12,14). In the three-dimensional structure of dephosphorylated IDH serine 113 is found in a pocket containing a number of positively charged and other polar residues which show a high degree of sequence conservation with isopropylmalate dehydrogenase (7). Although not yet solved with bound ligands, sequence conservation and charge distribution suggest that this pocket is the active site (7). Inactivation of IDH by phosphorylation occurs by preventing isocitrate from binding (15). Previous studies demonstrated that inhibition of binding is caused by the introduction of a negative charge at position 113 (14). These finding raise the question as to whether the mechanism of inactivation is through a direct electrostatic interaction between the phosphoserine and the negatively charged substrate isocitrate, or if it is mediated by an induced conformational change. To address this question, we determined the structure of phosphorylated IDH and compared it to the structure of the dephosphorylated enzyme.

EXPERIMENTAL PROCEDURES

IDH was phosphorylated *in vitro* by IDH kinase/phosphatase as described by LaPorte and Koshland (6) and crystals were grown essentially as for dephosphorylated IDH (7), except at 30 % saturated ammonium sulfate instead of 34 %. These grew to a size of 0.5 mm along the largest dimension and were isomorphous with the dephosphorylated crystals. Diffraction data were collected at room temperature on a Nicolet area detector using a laboratory Cu Kα rotating anode x-ray source and reduced with the XENGEN data reduction package.

The structure of phosphorylated IDH was determined by Fourier difference syntheses, using the dephosphorylated IDH model (7) as a parent structure. After the addition of water molecules placed in electron density at sites within 3.5 Å of potential hydrogen bond forming groups, the parent structure was refined using minimization with XPLOR (16). A total of 72 water molecules with B-factors less than 40 have been kept in the current model, where $B = 8\pi<u^2>_{rms}$, and u is the displacement of an atom about its equilibrium position. Covalently bound phosphate was located at serine 113 in $(F_{pho}-F_c)\alpha_{calc}$ and $(F_{pho}-F_{depho})\alpha_{calc}$ Fourier syntheses, with phases and amplitudes calculated from the dephosphorylated model. Phosphoserine was built into $(2F_o-F_c)\alpha_{calc}$ electron density with FRODO (17). The phosphorylated IDH model was refined with an effective solvent screening function of 20, to avoid an effect due to the lack of a solvation term in the empirical potential energy function used by XPLOR in which polar side chains with large B-factors form hydrogen bonds or salt bridges with nearby groups, although the electron density clearly indicates that these side chains project into the solvent. The net charge on the phosphoserine was set to zero, as with other charged groups. Water 545, displaced by the covalently bound phosphate group, was removed from the model prior to refinment with XPLOR. The R-factor of the phosphorylated model prior to refinement was 22.0 %. Residues 3 and 4, which had not been placed in the parent structure, were located in electron density for the phosphorylated structure, probably due to the improved data for phosphorylated IDH. The phosphorylated structure was refined for four rounds of alternating minimization and manual rebuilding with the use of both $(F_o-F_c)\alpha_{calc}$ and $(2F_o-F_c)\alpha_{calc}$ Fourier syntheses. As the final phosphorylated structure appeared to be superior in quality to the parent model, the phosphoserine was replaced by serine, water 545 was put back in the model, and this structure was refined for two rounds of minimization and rebuilding against dephosphorylated amplitudes to produce an improved dephosphorylated IDH structure. Crystallographic statistics are summarized in table I.

RESULTS

The rms positional change for all main chain atoms (including C_β) between the two structures is 0.11 Å, less than the error in coordinates of either structure, estimated at 0.20 Å rms for C_α positions by the empirical formula $\Delta r = 0.5Rr$ of Stroud, where R is the crystallographic R-factor and r is the maximum resolution in angstroms (a further discussion of this formula will be published elsewhere). The mean coordinate error is approximately 0.40 Å for all atoms by the method of Luzzati (18). As the two structures were not solved independently, it is expected that the mean atomic shift is less than the mean coordinate error. The only significant positional changes are in the immediate vicinity of the phosphorylation site, as seen in Fig. 2. The conserved tyrosine 160 rotates by 15° about its C_α-C_β bond, causing the hydroxyl oxygen to move by 0.9 Å, the largest movement of any protein atom. Isoleucine 159 moves by up to 0.3 Å (at $C_{\gamma 2}$), largely as a result of change in main-chain torsion angles, and loop 229-234 undergoes a small concerted shift, with displacements of 0.1 to 0.6 Å. The entire loop undergoes a mean shift of 0.16 Å in the same direction, with an rms shift of 0.25 Å from the dephosphorylated structure. These movements appear to accommodate the new position of tyrosine 160. These changes, although similar in size or smaller than the estimated coordinate error, are clearly seen in $(F_{pho}\text{-}F_c)\alpha_{calc}$ and $(F_{pho}\text{-}F_{depho})\alpha_{calc}$ difference maps.

Lysine 199, which points into a large internal solvent-filled channel between the small and the clasp-like domains of IDH, and is in contact with the loop 229-234, also moves by up to 0.3 Å. This internal solvent pocket separates the phosphorylation sites on the two subunits, but displaced residues surrounding each phosphorylation site do not approach each other by less than 4.0 Å. Packing in and around the internal solvent-filled channel appears too loose to transmit a conformational change from one phosphorylation site to the other. This is in accord with the absence of cooperativity in the kinetics for phosphorylation of IDH by IDH kinase/phosphatase (6). Water 545 is replaced by the covalently bound phosphate, and there is a local rearrangement of water structure in the vicinity of residue 113. Water 417 moves by 1.5 Å; that this is the "same" water in both structures is signified by its unusually low B-factor of 10 and 11 in the phosphorylated and dephosphorylated structures, respectively. The identity of 417 is not well established, but is modeled more reasonably as a water than as any of the ionic species (ammonium, sulfate, citrate, phosphate, sodium, chloride) present. The movement of water 417 closer to the covalently bound phosphate (from 3.9 to 3.4 Å) also brings it nearer to tyrosine 160 (from 4.2 to 3.6 Å) and may initiate the other small conformational changes.

Structural changes are highly localized in the region of the phosphorylation site (Fig.s 3, 4). Aside from the atoms mentioned above, near serine 113, no protein atom moves more than 0.4 Å. The pattern of atomic shifts between the two structures does not increase with B-factor (Fig. 5), hence does not follow the pattern expected for shifts due to random positional errors (a general discussion of mean shift distributions and coordinates errors will be published elsewhere). The observation that there is actually a decrease in shift with increasing B-factor is due to the relatively low average B-factor in the region of serine 113.

DISCUSSION

Because of the central importance of protein phosphorylation in biological regulatory systems, much effort has been invested in understanding how such covalent modifications alter protein function. In glycogen phosphorylase (GP), phosphorylation of serine 14 initiates the GPb to GPa transition, in which long-range conformational changes occur (5). In this transition, the thermodynamic equilibrium between conformational states along the activation pathway of the enzyme is shifted to more active conformations, through effects both at distant allosteric effector sites and at the active site. In contrast to GP, which is activated by long-range conformational changes initiated by phosphorylation or allosteric effectors, IDH is inactivated by phosphorylation through an effect on substrate binding without any such long-range changes.

The location of the phosphorylation site in a pocket lined with highly conserved polar side chains, and the lack of a large-scale conformational change in the unliganded enzyme on phosphorylation, suggest IDH is inactivated by a direct electrostatic isocitrate-phosphoserine interaction. Alternatively, in the absence of a large conformational change upon phosphorylation, inactivation of IDH might proceed through small conformational changes if they were of sufficiently large energy. Another possibility is that phosphorylation may prevent an induced conformational change necessary for substrate binding.

It may be asked whether lattice forces have prevented a solution-state conformational change involved in inactivation. Crystal packing interactions have occasionally had significant effects on protein structures. As phosphorylation reduces activity by at least three orders of magnitude (14), inactivation involves a free energy change of at least 4.5 kcal/mol. The lattice interaction energy is likely to be small in crystals of IDH, as these crystals are quite unstable, dissolving rapidly if placed in the well solution used in crystallization. It is thus likely that the free energy difference involved in inactivation is therefore substantially larger than the lattice interaction energy, hence unlikely that the absence of a conformational change is an artifact of the crystalline state.

The structure of phosphorylated isocitrate dehydrogenase demonstrates that an enzyme can be phosphorylated in a functionally relevant way without a long-range conformational change. Thus the repertoire of known structural effects of regulatory covalent modification is increased. The diversity of possible structural effects of reversible covalent modifications of proteins produced by evolution is undoubtedly related to the great diversity of biological function of these modifications.

References

1. Krebs, E. (1986) *The Enzymes* **17**:3-18.

2. Edelman, A.M., Blumenthal, D.K. and Krebs, E.G. (1987) *Ann. Rev. Biochem.* **56**:567-613.

3. Wang, J.Y.J. and Koshland, D.E., Jr. (1978) *J. Biol. Chem.* **253**, 7605-7608.

4. Garnak, M. and Reeves, H.C. (1979) *J. Biol. Chem.* **254**, 7915-7920.

5. Sprang, S.R., Fletterick, R.J., Goldsmith, E.J., Madsen, N.B., Acharaya, K.R., Stuart, D.J., Varvill, K. and Johnson, L.N. (1988) *Nature* **336**, 215-221.

6. LaPorte, D.C. and Koshland, D.E., Jr. (1983) *Nature* **305**, 286-290.

7. Hurley, J. H., Thorsness, P.E., Ramalingam, V., Helmers, N.H., Koshland, D.E., Jr. and Stroud, R.M. (1989) *Proc. Natl. Acad. Sci. USA* **86**, 8635-8639.

8. Kornberg, H.L. and Madsen, N.B. (1957) *Biochim. Biophys. Acta* **24**, 651-653.

9. Kornberg, H.L. (1966) *Biochem. J.* **99**, 1-11.

10. Holms, W.H. and Bennett, P.M. (1971) *J. Gen. Microbiol.* **65**, 57-68.

11. Wang, J.Y.J. and Koshland, D.E., Jr. (1982) *Arch. Biochem. Biophys.* **218**, 59-67.

12. Borthwick, A.C., Holms, W.H. and Nimmo, H.G. (1984) *Biochem. J.* **222**, 797-804.

13. LaPorte, D.C., Walsh, K. and Koshland, D.E., Jr. (1984) *J. Biol. Chem.* **259**, 14068- 14075.

14. Thorsness, P.E. and Koshland, D.E., Jr. (1987) *J. Biol. Chem.* **262**, 10422-10425.

15. Dean, A.M, Lee, M.H.I. and Koshland, D.E., Jr. *J. Biol. Chem.* **264**, 20482-20486.

16. Brunger, A.T., Kuriyan, K. and Karplus, M. (1987) *Science* **235**, 458-460.

17. Jones, T.A. (1985) *Methods Enzymol.* **115**, 157-170.

18. Luzzati, P.V. (1952) *Acta. Crystallogr.* **5**:802-810.

Figure and Table Legends

Figure 1. Region of residue 113 in positive difference electron density from a 2.5 Å $(F_o-F_c)\alpha_{calc}$ electron density map based on phases and amplitudes calculated from the dephosphorylated IDH model (7) and observed amplitudes for phosphorylated IDH. The largest peak, with a peak height of 20 standard deviations, is for the covalently bound phosphate at residue 113; the other major peak seen represents the displacement of water 417.

Figure 2. The environment of residue 113 viewed looking into the front pocket of IDH. Phosphorylated IDH is shown with solid bonds, and dephosphorylated IDH with open bonds. Portions of both subunits in the dimer are shown. Only water molecules which move by more than 0.2 Å between the two forms of IDH are shown. Waters of phosphorylated IDH are filled black, and waters of dephosphorylated IDH are open. Labelled residues include the conserved residues aspartates 283' (the prime indicates the second subunit), 307 and 311; arginines 119, 129, 153; glutamate 336; tyrosine 160 and lysine 230'. Also labelled are arginine 112, serine 113, and water 417.

Figure 3. Mean atomic shift between the two forms of IDH as a function of distance to phosphoserine 113 P in phosphorylated IDH. Shifts are plotted against the distance to the nearest of the two phosphorylation sites (one per subunit) in the IDH dimer. The mean shift rapidly decreases with

distance from the phosphorylation site, approaching the overall value for the entire molecule at 10 Å from site 113.

Figure 4. Mean atomic shift between the two forms of IDH averaged over eight residues as a function of residue number. Shifts are plotted against the central residue in the window of averaging. The largest shifts are restricted to the regions of residues 113, 160 and 234, close to the phosphorylation site in three-dimensional space.

Figure 5. Mean atomic shift between the two forms of IDH as a function of B-factor. B-factors are taken from the phosphorylated structure, but are similar in both structures. The decrease in the mean shift with B-factor is contrary to the expected pattern for a distribution of changes due to random positional errors.

Table 1. Crystallographic statistics for phosphorylated IDH (P-IDH) and dephosphorylated IDH (IDH). The crystallographic R-factor, $R_c = \Sigma|F_o - F_c|/\Sigma F_o$ is summed over all reflections with $|F|/\sigma(F) > 1$ from 5 to 2.5 Å; F_o and F_c are the observed and calculated amplitudes. $R_{merge} = \Sigma|I_i - \langle I\rangle|/\Sigma\langle I\rangle$, summed over all observations to 2.5 Å from four crystals.

Crystallographic Statistics for IDH

Space Group $P4_32_12$ a=b=105.1 Å c=150.3 Å Resolution 2.5 Å

	Reflections collected	Reflections $F/\sigma(F) > 1$	Observations collected	Rmerge	Rc
P-IDH	29667	21162	156365	.121	.169
IDH	27951	19945	119034	.124	.180

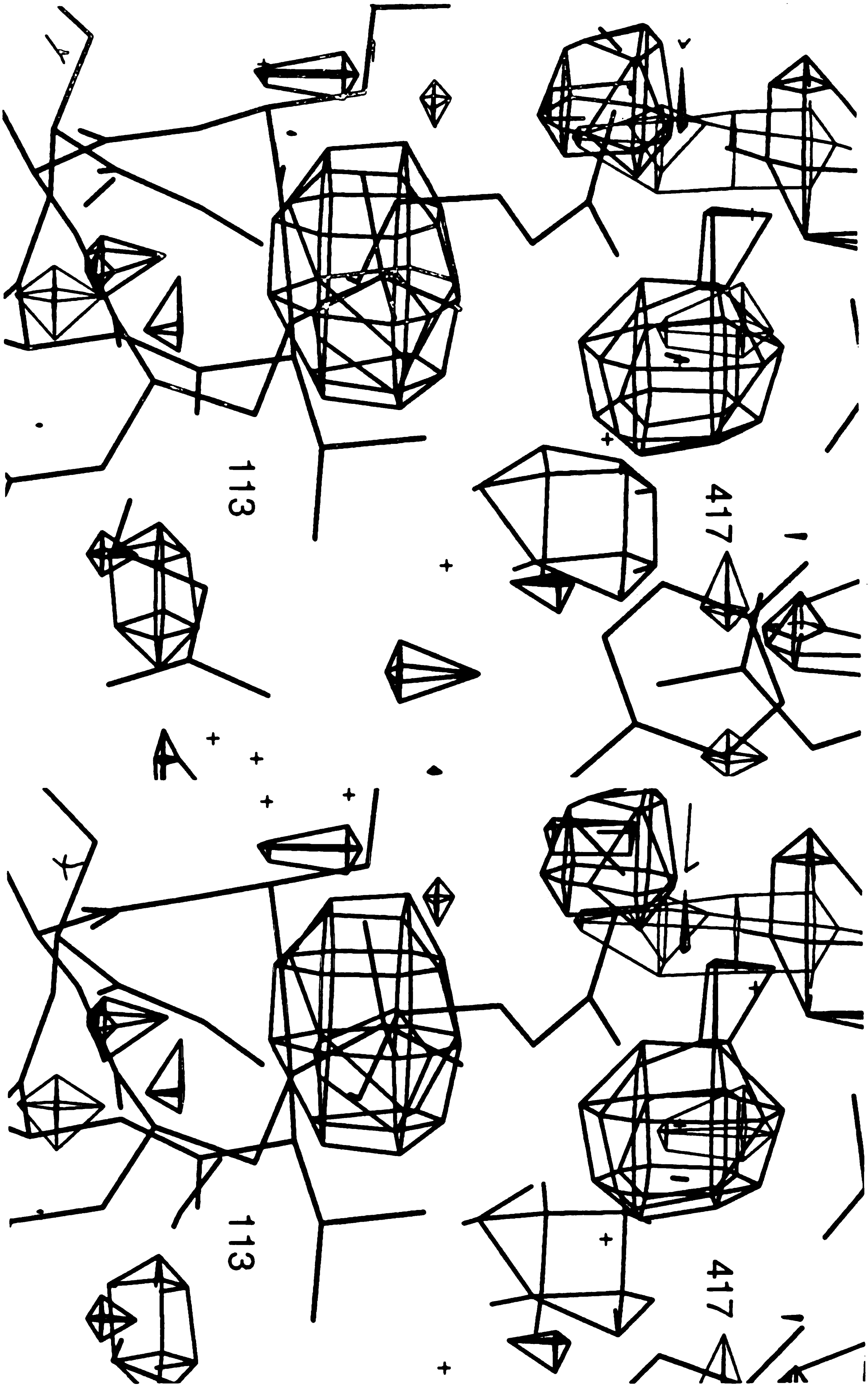
A

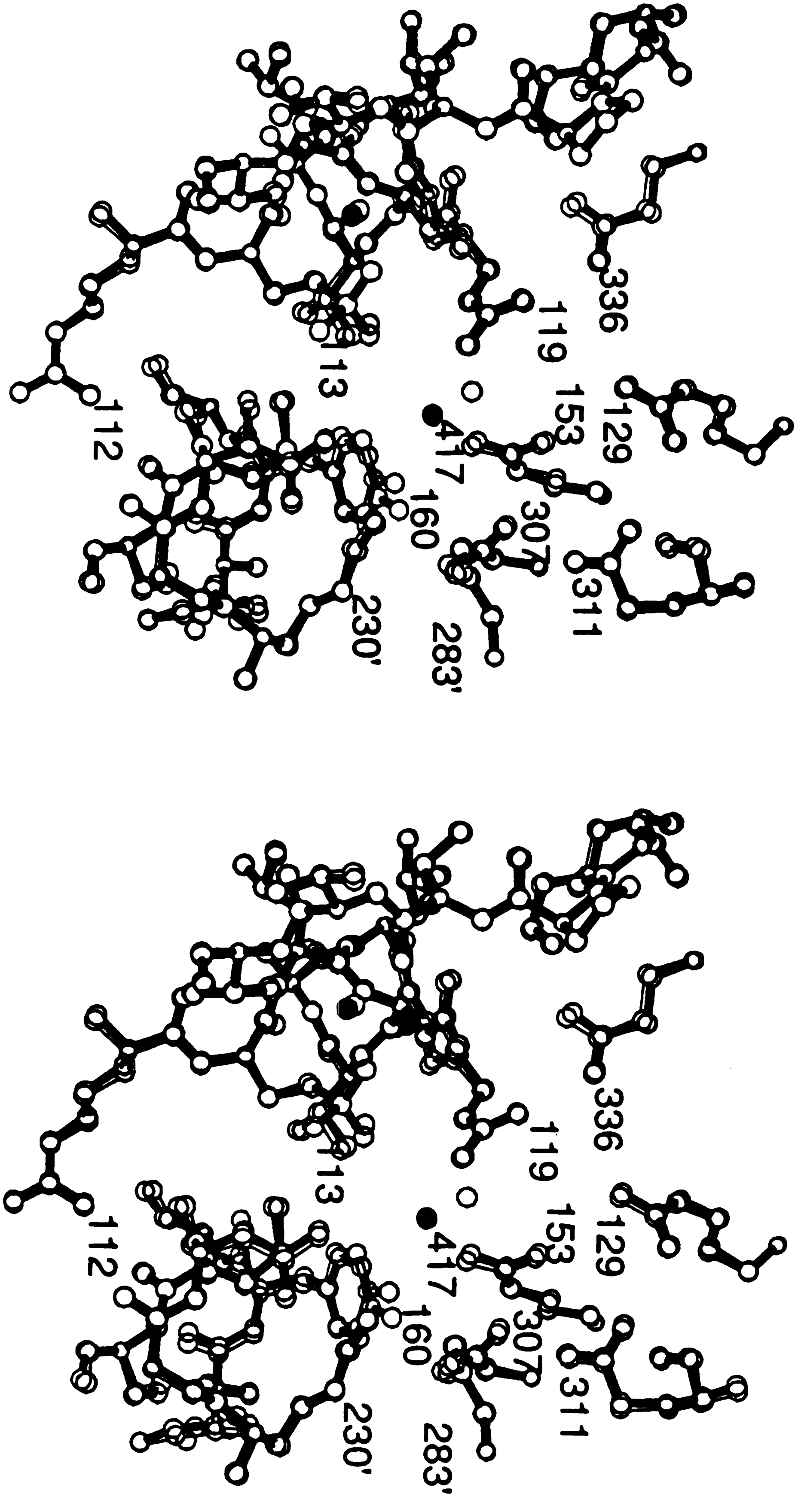

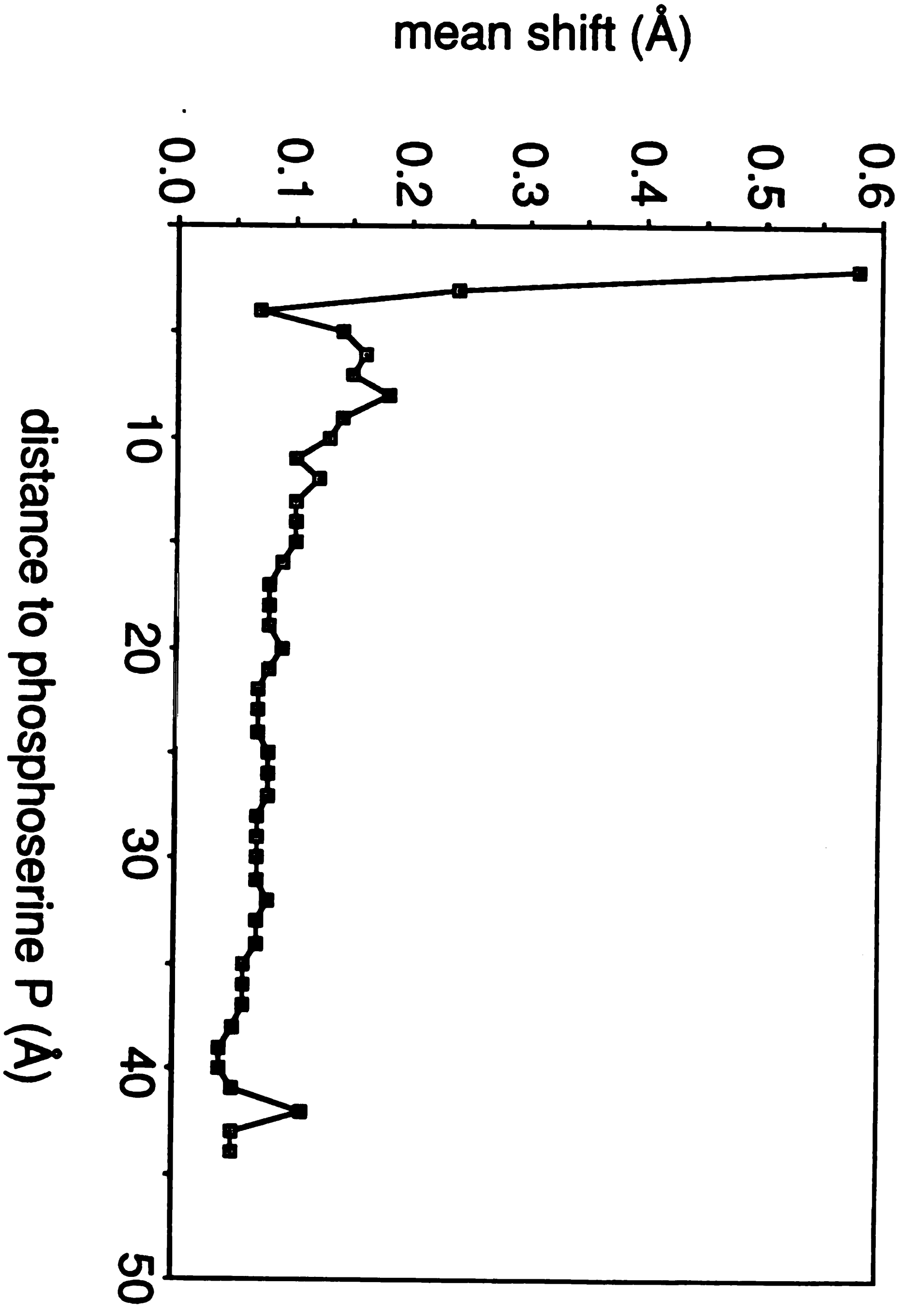
mean shift (Å)
0.0
0.1
0.2
0.3
0.4
0.5
0.6
10
20
30
40
50
distance to phosphoserine P (Å)

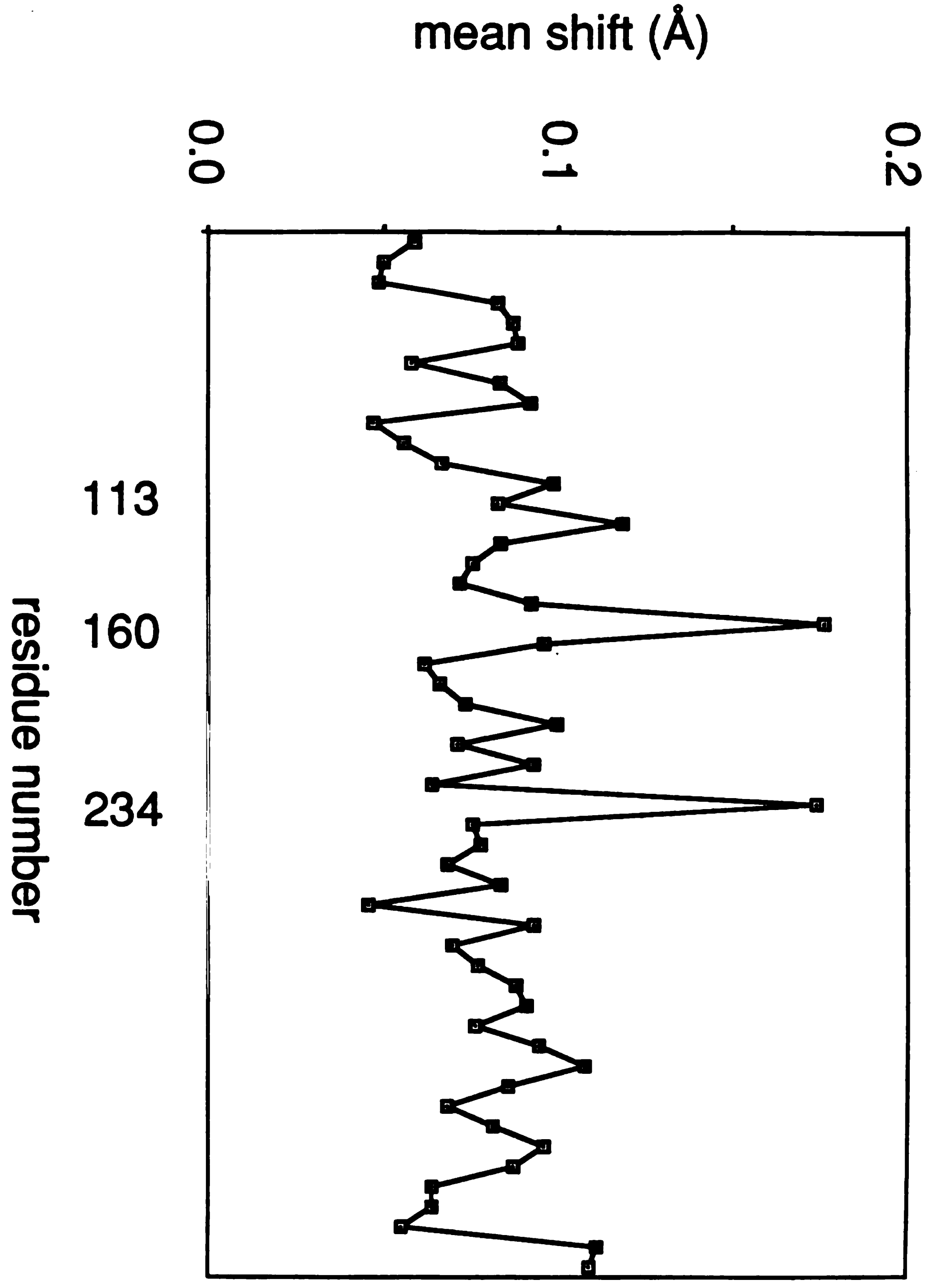
mean shift (Å)
0.0
0.1
0.2
113
160
234
residue number

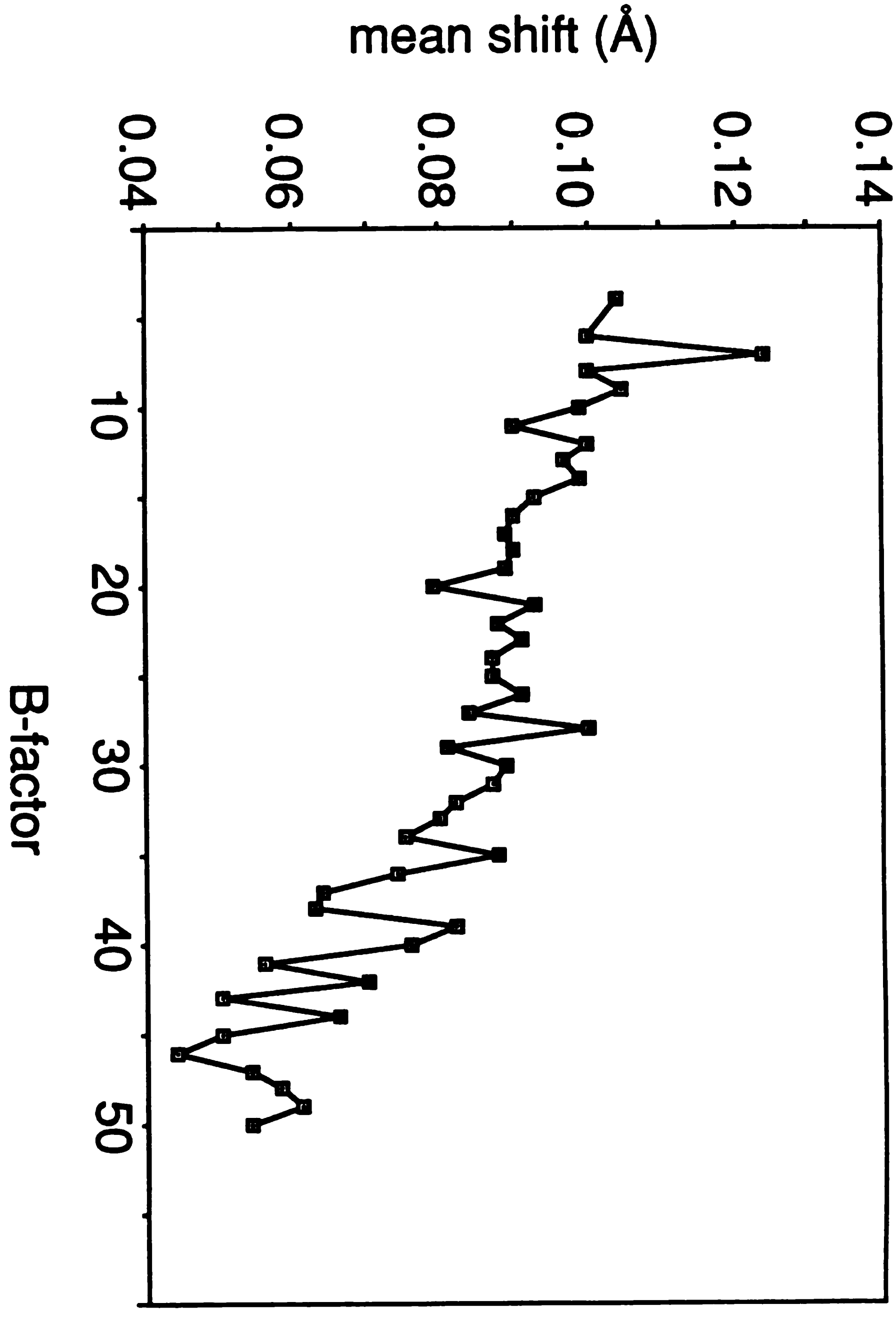
mean shift (Å)
0.04
0.06
0.08
0.10
0.12
0.14
10
20
30
40
50
B-factor

Regulation of an enzyme by phosphorylation at the active site

James H. Hurley, Antony M. Dean, Julie L. Sohl, Daniel E. Koshland, Jr., and Robert M. Stroud

J. H. Hurley, J. L. Sohl, and R. M. Stroud, Dept. of Biochemistry and Biophysics and Graduate Group in Biophysics, University of California at San Francisco, San Francisco, Ca. 94143-0448

A. M. Dean and D. E. Koshland, Jr., Dept. of Molecular and Cell Biology, University of California at Berkeley, Berkeley, Ca. 94720

The isocitrate dehydrogenase of *Escherichia coli* is regulated by phosphorylation at serine 113, which inactivates the enzyme by inhibiting isocitrate binding. In the three-dimensional structure of the enzyme-substrate complex, isocitrate is hydrogen bonded to serine 113. The structures of inactive mutants in which aspartate and glutamate replace serine 113 show no detectable conformational changes from wild-type, indicating structural changes are not required for inactivation. Calculations based on the structure of a magnesium-isocitrate complex with the glutamate 113 mutant show that the change in electrostatic potential upon introduction of a negative charge by either phosphorylation or site-directed mutagenesis is sufficient to inactivate the enzyme.

Phosphorylation, the most common regulatory post-translational modification of proteins, is of central importance in metabolism, signal transduction, and many other cellular processes (1). Yet the three-dimensional structures of both the phosphorylated and dephosphorylated states are available for only two enzymes, glycogen phosphorylase (2) and isocitrate dehydrogenase (IDH) (*threo*-Ds-isocitrate:NAD(P)$^+$ oxidoreductase [decarboxylating]; E. C. 1.1.1.42) (3,4). Phosphorylation of glycogen phosphorylase enhances activity by means of long-range conformational changes (2). An understanding of the structural basis of a very different response in isocitrate dehydrogenase, complete inactivation by phosphorylation (5), has been hindered by the lack of knowledge of the active site. In order to determine the active site and its relationship to the phosphorylation site, and to account for the effect of introducing a negative charge at the phosphorylation site, the structure of a complex of dephosphorylated IDH with magnesium isocitrate was determined.

Inactivation by phosphorylation of Ser^{113} in IDH is mimicked upon substituting aspartate (6) or glutamate (8) at this site. In both cases the binding of isocitrate is inhibited (7,8). To clarify the mechanism of inactivation, the three-dimensional structures of the unliganded S113D mutant (6) and the S113E mutant (8) in both the unliganded and substrate-bound states were determined and compared with those of the phosphorylated and dephosphorylated enzymes.

To obtain a crystalline complex of IDH with substrate, IDH crystals (3) were soaked in ligand-containing solutions. In order to determine unambiguously the metal binding site, x-ray reflection data were collected (3) to 2.5 Å resolution both for crystals soaked in Mg^{++} and Mn^{++} containing solutions (Table 1). The metal ion was located at the largest peak (11 σ) in an $(F_o(Mn)-F_o(Mg))\alpha_{calc}$ Fourier difference map, with phases calculated from the refined structure of free IDH. $(F_o(Mn)-F_o(Free))\alpha_{calc}$ and $(F_o(Mg)-F_o(Free))\alpha_{calc}$ difference maps showed a large negative peak (-16 σ) at the position of water 417 in the free enzyme, indicating that this water was displaced in the substrate-bound enzyme. Water 417 was removed and the Mg^{++} ion was placed at the major peak in the $(F_o(Mn)-F_o(Mg))\alpha_{calc}$ Fourier difference map (Fig. 1). Prior to refinement, an R-factor of 0.239 was calculated with respect to amplitudes for the Mg isocitrate complex. This model was then refined (9) to an R-factor of 0.184. R,S-isocitrate, the biologically relevant isomer (11), was placed in an $(F_o(Mg)-F_c)\alpha_{calc}$ difference map with amplitudes and phases calculated from the refined Mg complex model, and the model was refined to a final R-factor of 0.176. The S113D and S113E mutants were crystallized as for wild-type (3) and data was collected in the absence of ligands. The aspartate and glutamate side chains were located in $(F_o(mutant)-F_o(wt))\alpha_{calc}$ difference map with phases calculated from wild type and the structures were refined to final R-factors of 0.163 at 2.8 Å and 0.179 at 2.4 Å, respectively. Crystals of the S113E mutant were soaked in the same Mg^{++} isocitrate containing solution used to obtain the wild-type enzyme-substrate complex. The S113E enzyme-substrate complex model was built starting from models for free S113E and the wild-type complex, adjusted with the aid of $(F_o(\mathrm{S113E\ complex})-F_c(\mathrm{S113E\ free}))\alpha_{calc}$ and $(F_o(\mathrm{S113E\ complex})-F_c(\mathrm{wt\ complex}))\alpha_{calc}$ difference maps, and refined to an R-factor of 0.168 at 2.5 Å.

Isocitrate binds in a pocket between the two major domains of IDH, in which both subunits of the dimer participate (Fig. 2). Hydrogen bonds are formed between isocitrate and Ser^{113}, Arg^{119}, Arg^{129}, Arg^{153}, Tyr^{160}, $\mathrm{Lys}^{230'}$ (the ' indicates the second subunit), and two bound water molecules. Mg^{++} is coordinated by isocitrate, $\mathrm{Asp}^{283'}$, Asp^{307}, and two bound water molecules in a roughly octahedral manner. The coordination of Mg^{++} to the α-carboxylate and the hydroxyl oxygen O7 of isocitrate positions the metal ion to play the key role in catalysis (to be discussed elsewhere). Structural changes from the unliganded enzyme are local, the largest being movements of the side chains of Arg^{119} and Arg^{129} by up to 2.1 Å in which the guanidino groups approach each other and the isocitrate molecule more closely (Fig. 3).

The structures of the Asp^{113} and Glu^{113} mutants show essentially no structural differences from wild-type IDH, indicating that structural changes are not required for inactivation. The movements of Tyr^{160} and Wat^{417} observed in phosphorylated IDH do not occur in S113D and S113E. Tyr^{160} and Wat^{417} occupy positions in the S113D and S113E structures of IDH more similar to the free form than the phosphorylated or substrate-bound forms. In contrast to results reported for HPr (12), in which similar shifts in two-dimensional NMR spectra indicated similar structural changes on phosphorylation or Ser to Asp replacement, structural changes on phosphorylation of IDH are not mimicked by the S113D replacement. The hydroxyl oxygen of Tyr^{160} in phosphorylated IDH is 0.5 Å from the same atom in the substrate-bound structure, but 0.9 Å away from this atom in the S113D and free structures. The observation that the conformation of Tyr^{160} in the substrate-bound form is most similar to that in the phosphorylated form indicates that small conformational changes seen on phosphorylation (4) are inessential for regulation.

The relative activities of uncharged site-directed mutants at position 113 (6,7,8) can be explained by the observation that the phosphorylatable serine forms a hydrogen bond with isocitrate. Threonine and alanine are the least disruptive replacements, with affinity for isocitrate decreased 2- to 3-fold relative to wild-type, respectively (6). Threonine can still hydrogen bond, but must rotate due to steric hindrace of $C\gamma$ by Val^{116}, moving the hydroxyl to a less favorable position. Alanine cannot form a hydrogen bond, but may accommodate a water molecule near the position occupied by $O\gamma$ of serine in wild-type IDH. Cysteine, with affinity for isocitrate reduced 9-fold, is likely to be sterically unfavorable for isocitrate binding because of the bulk of the sulfhydryl group. Tyrosine, with 115-fold decreased affinity for isocitrate, will require some adjustment of the main chain and surrounding regions in the unliganded enzyme, and is also likely to be sterically unfavorable for isocitrate binding. Lysine, with 80-fold decreased affinity for isocitrate, is likely to be sterically unfavorable. Based on relative K_m values for mutants at residue 113 (8), the loss of the hydrogen bond with Ser^{113} corresponds to a reduction in affinity for isocitrate with $\Delta(\Delta G_{bind}) = 0.4$ kcal/mole. Steric disruption of binding by lysine and tyrosine side chains, comparable in size to a serine phosphate, account for an additional reduction in affinity of $\Delta(\Delta G_{bind})$ = 2.3 to 2.5 kcal/mole. After a steric contribution of 2.5 kcal/mole is substracted, the electrostatic component of $\Delta(\Delta G_{bind})$ must be at least 0.8 kcal/mole for S113D, and is probably substantially greater, as the aspartate side-chain is less bulky than tyrosine or lysine.

Despite the very low affinity of the S113E mutant for isocitrate at physiological pH and ionic strength, isocitrate binds to this mutant at the low pH (6.0), high ionic strength (6.9 M), and high isocitrate concentration (100 mM) used to obtain a crystalline complex. Isocitrate is sterically accommodated in the active site by movements of up to 1.6 Å of both the Glu^{113} side chain and the γ-carboxylate of isocitrate (Fig. 3). The γ-carboxylate becomes poorly ordered in the S113E complex, with B-factors increasing from 32-38 in the wild-type complex to 45-50. O4 of isocitrate is within 3.0 Å of Glu^{113} in the complex, but the geometry is not favorable for formation of a hydrogen bond by a protonated form of either isocitrate or Glu^{113}. The unfavorable geometry for isocitrate binding in the active site of S113E may reflect a reduced affinity for the substrate even under conditions in which the role of electrostatic interactions is minimal.

To determine whether an electrostatic interaction could account for the effect of introducing a negative charge at position 113, we used numerical solution of the Poisson-Boltzmann equation (13) to calculate the change in the electrostatic free energy of binding of the Mg^{++} isocitrate complex produced by either phosphorylation or replacement of serine by aspartate. Magnesium and isocitrate bind to $NADP^+$-dependent IDH as a complex (14). Calculations were based on the structure of the S113E enzyme-substrate complex. Model structures of phosphorylated IDH and S113D complexed with isocitrate were also built based on the structures of substrate-bound wild-type IDH, and phosphorylated IDH and S113D in the absence of substrate. When the Mg^{++} isocitrate structure is superimposed on the phosphorylated IDH and S113D structures to construct a model complex, distances from the γ-carboxylate of isocitrate to the nearest phosphate or carboxylate oxygen of residue 113 are less than 2.4 Å. When rotations in main-chain and side-chain torsion angles for residue 113 are allowed, in a manner similar to that seen in the crystal structure of the S113E complex, a complex with either the phosphorylated or S113D enzymes can be accommodated without unreasonably close contacts.

The calculated change in electrostatic free energy of binding of Mg^{++} isocitrate to S113E is $\Delta(\Delta G_{bind}) = +21$ kcal/mole (Table 2). Calculations were repeated for alternative model-built structures to determine the dependence of $\Delta(\Delta G_{bind})$ on structural changes. Models A, B, and C are based on maximal shifts of residue 113 or isocitrate which move negative charges as far apart as possible, rotating only the γ-carboxylate of isocitrate and the main chain and side chain at residue 113. $\Delta(\Delta G_{bind})$ is +5 to +13 kcal/mole in alternate models for phosphorylated IDH and S113D. These calculations, although dependent on the use of the linearized Poisson-Boltzmann equation and the assumption that the polarizability of the protein interior is homogenous and isotropic, show that the change in electrostatic potential can account for the large observed decrease in affinity for isocitrate.

The increase in $\Delta(\Delta G_{bind})$ for fully ionized isocitrate binding to IDH with an ionized aspartate or serine phosphate is so large that it must be asked whether a low level of activity contributed by the protonated forms of Asp^{113}, phospho-Ser^{113}, or isocitrate could be significant. In a calculation based on the crystallographic structure of S113D the pK_a of Asp^{113} was lowered by one unit, to 2.9. The fraction of S113D IDH protonated at Asp^{113} at pH 7.5 is thus less than 2.5×10^{-5}, consistent with inactivation. A similar calculation for phosphorylated IDH shows the intrinsic pK_a values of phospho-Ser^{113} of roughly 1.0 and 6.3 are lowered to -1.4 and 4.6. The fraction of phospho-Ser^{113} singly protonated at pH 7.5 is thus less than 10^{-3}. Since one negative charge is still present, $\Delta(\Delta G)$ for isocitrate binding due to the singly ionized species is one half the value calculated for the doubly ionized serine phosphate in the linear Poisson-Boltzmann equation. Based on the potential change calculated for model C, the calculated upper limit on relative binding contributed by a singly protonated serine phosphate is less than 1.8×10^{-5} at pH 7.5, again consistent with inactivation. The tribasic metal-isocitrate complex is the principal substrate of $NADP^+$-dependent IDH. Protonated forms of isocitrate are believed to be kinetically unimportant under normal circumstances (14), but the metal-isocitrate complex has a pK_a of 5.7 (14), and it is likely that a singly protonated metal-isocitrate complex accounts for the low level of activity (8) remaining for the S113D and S113E enzymes.

In contrast to the only other well-characterized mechanism for regulation by phosphorylation, IDH demonstrates that phosphorylation can act directly at a substrate binding site without inducing large structural changes. Electrostatic potential calculations based on the structure of the enzyme-substrate complex and comparison to results of site-directed mutagenesis lead to the conclusion that the loss of a hydrogen bond with isocitrate and a combination of electrostatic and steric interactions between the serine phosphate and isocitrate are responsible for inhibition of the enzyme.

1. E. Krebs, in *The Enzymes* (P. D. Boyer and E. G. Krebs, eds) 3rd Ed., Vol. 17 pp. 3-18, Academic Press, New York (1986); A. M. Edelman, D. K. Blumenthal and E. G. Krebs, *Ann. Rev. Biochem.* **56**:567 (1987).

2. S. R. Sprang, K. R. Acharaya, E. J. Goldsmith, D. I. Stuart, K. Varvill, R. J. Fletterick, N. B. Madsen and L. N. Johnson, *Nature* **336**:215 (1988); E. J. Goldsmith, S. R. Sprang, R. Hamlin, N.-H. Xuong, R. J. Fletterick, *Science* **245**:528 (1989); D. Barford and L. N. Johnson, *Nature* **340**:609 (1989).

3. J. H. Hurley, P. E. Thorsness, V. Ramalingam, N. H. Helmers, D. E. Koshland, Jr. and R. M. Stroud, *Proc. Natl. Acad. Sci. USA* **86**:8635 (1989).

4. J. H. Hurley, A. M. Dean, P. E. Thorsness, D. E. Koshland, Jr., and R. M. Stroud, *J. Biol. Chem.* **265**:3599 (1990).

5. D. C. LaPorte and D. E. Koshland, Jr., *Nature* **305**:286 (1983).

6. P. E. Thorsness and D.E . Koshland, Jr., *J. Biol. Chem.* **262**:10422 (1987).

7. A. M. Dean, M. H. I. Lee and D. E. Koshland, Jr., *J. Biol. Chem.* **264**:20482 (1989).

8. A. M. Dean and D. E. Koshland, Jr., submitted to *Science*. For IDH mutants, the assumption that K_m and K_d for isocitrate are similar appears justified, hence the relative K_m for isocitrate is used to estimate $\Delta(\Delta G_{bind})$.

9. A. T. Brunger, K. Kuriyan and M. Karplus, *Science* **235**:458 (1987).

10. B. R. Brooks, R. E. Bruccoleri, B. D. Olafson, D. . States, S. Swaminathan, and M. Karplus, *J. Comp. Chem.* **4**:187 (1983).

11. D. van der Helm, J. P. Glusker, C. K. Johnson, J. A. Minkin, N. E. Burow and A. L. Patterson, *Acta Crystalogr. Sect. B.* **24**:578 (1968).

12. M. Wittekind, J. Reizer, J. Deutscher, M. H. Saier, and R. E. Klevit, *Biochemistry* **28**:9908 (1989).

13. I. Klapper, R. Hagstrom, R. Fine, K. Sharp and B. Honig, *Proteins* **1**:47 (1986); M. K. Gilson, K. A. Sharp, and B. H. Honig, *J. Comp. Chem.* **9**:327 (1988).

14. J. J. Marr and M. M. Weber, *Arch. Biochem. Biophys.* **158**:782 (1973): data for NADP$^+$-dependent IDH from *Salmonella typhimurium*. R. S. Ehrlich and R. F. Colman, *Biochemistry* **26**:3461 (1987); R. S. Ehrlich and R. F. Colman, *Biochemistry* **28**:2058 (1989): data for NADP$^+$-dependent IDH from pig heart; the pK$_a$ value is for Cd^{++} isocitrate.

15. We thank Kim Sharp, Anthony Nicholls, and Barry Honig for use of their program DELPHI; Peter Thorsness for assistance in preparing S113D IDH; Brian Shoichet for assistance with obtaining small molecule structures; and Joe Day for helpful discussions of protein-metal interactions. This work was supported by grants GM 24485 from the National Institutes of Health to R. M. S., 04200 from the National Science Foundation to D. E. K., a grant from the Lucille Markey Foundation to D. E. K., a U.C. Regent's fellowship to J. H. H, and a National Science Foundation fellowship to J. L. S. Crystallographic refinement was carried out at the Pittsburgh Supercomputer Center under grant DMB890040P. Coordinates for the Mg^{++} isocitrate complex and the S113D and S113E mutants will be deposited with the Protein Data Bank at Brookhaven.

Table 1

All x-ray intensity data were collected with a Nicolet area detector and reduced with the XENGEN package. Structures were refined with XPLOR minimization (9) and manual rebuilding into (2Fo-Fc)αcalc electron density maps. Energy parameters were obtained from the CHARMM library (10) normally used with XPLOR, except van der Waals parameters were added for Mg^{++} and improper angles for the two chiral centers of isocitrate were calculated from the small molecule structure (11). $R_{cryst} = \Sigma|F_o - F_c|/\Sigma F_o$, summed over reflections with $|F|/\sigma(F) > 1$. $R_{merge} = \Sigma|I_i - \langle I\rangle|/\Sigma\langle I\rangle$, summed over all observations from all crystals. * Data was collected for only one crystal each for the Mn^{++} complex and both S113E structures; three crystals each were used for collection of the other two data sets. Reflections with $F/\sigma(F)>1.0$ with a low-resolution cut-off of 5.0 Å were used in refinement and R-factor calculation.

Table 2

Electrostatic potential changes $\Delta\Phi$ at each fully charged atom in the Mg^{++} isocitrate complex, and the change in electrostatic free energy of binding for Mg^{++} isocitrate $\Delta(\Delta G_{bind})$, between each model and the wild-type dephosphorylated enzyme. $\Delta(\Delta G_{bind}) = \Sigma q_i \Delta\Phi_i$, summed over all full charges in the Mg^{++} isocitrate complex. "Xtal" refers to the calculation based on the crystallographic structure of the Mg^{++} isocitrate complex with the S113E mutant. A and B are alternate models for a S113D mutant complex, C and D are alternate models for a phosphorylated IDH complex. To test the accuracy of the calculations and their sensitivity to variable parameters, a series of trial calculations were made. Our results were strongly dependent on the value of dielectric constant for the protein interior, so a value 4 was chosen, at the high end of the range 2-4 normally considered appropriate. A dielectric constant of 80 was used for the solvent region. Treatment of solvent screening proved essential to obtain reasonable results; when a dielectric constant of 4 and ionic strength I = 0.0 M were assigned to all space, the increase in binding energy calculated in model D was 51 kcal/mole, compared to 13.1 kcal/mole calculated with a solvent dielectric constant of 80 and non-zero I. The linearized Poisson-Boltzmann equation was used to calculate the potential due to the charges on Glu^{113}, Asp^{113}, or phospho-Ser^{113} alone. I = 0.115 M, the ionic strength of the buffer normally used for IDH activity assays; changing I to 0.145 M had a negligible effect. No ion exclusion layer was used for the calculations reported here, but the use of such a layer was found to have a minimal effect on the solution to the linear equation in trial calculations. Potentials were calculated by a three-step focussing procedure: the first calculation used a 6.25 Å grid spacing with Debye-Huckel boundary conditions, followed by calculations on grids with 1.25 and 0.625 Å spacings. Repeating the calculation on a 0.30 Å grid produced no further change in the result. The calculated $\Delta(\Delta G_{bind})$ was identical at 0.625 and 0.30 Å, and roughly 10 % larger at 1.25 Å. All calculations were performed on a cubic grid with 65 units per side and iterations continued to convergence. $\Delta(\Delta G_{bind})$ calculated from multiple cycles of translational averaging varied from the mean by less than 2 %. * $\Delta(\Delta G_{bind})$ = 21 kcal/mole ± 1 kcal/mole is obtained by averaging the calculated $\Sigma q_i \Delta \Phi_i$ = 22 kcal/mole for $\Delta \Phi_i$ at the Glu^{113} side chain due to charges on Mg^{++} isocitrate and the $\Sigma q_i \Delta \Phi_i$ = 20 kcal/mole for $\Delta \Phi_i$ at Mg^{++} isocitrate due to charges on

Glu^{113}. As these two quantities are formally equal, the discrepancy is a measure of error in the finite-difference solution to the Poisson-Boltzmann equation.

Figure 1

A. Isocitrate in electron density from a $(F_o(Mg)-F_c)\alpha_{calc}$ difference map at 2.5 Å resolution with amplitudes and phases calculated from a model refined after including Mg^{++} but not isocitrate. The map is contoured at 5 σ and superimposed on the refined model of the Mg^{++} isocitrate complex. X-ray intensity data were collected for IDH crystals soaked for at least three hours in freshly prepared solutions of 100 mM *threo*-Ds(+)-isocitric acid (monopotassium salt) obtained from Sigma, 10 mM of either $MgSO_4$ or $MnCl_2$, 100 mM NaCl, 35 mM Na_2HPO_4, 2 mM DTT and 0.02 % NaN_3 in 50 % saturated $(NH_4)_2SO_4$, with pH adjusted to 6.0 with concentrated NH_4OH. Local scaling was used for all map calculations. B. 2.8 Å resolution $(F_o(S113D)-F_o(\text{wild type}))\alpha_{calc}$ difference map, contoured at 3.5 σ and superimposed on the refined model of the S113D mutant. C. 2.5 Å resolution $(F_o(S113E)-F_o(\text{wild type}))\alpha_{calc}$ difference map, contoured at 5 σ and superimposed on the refined model of the S113E mutant.

Figure 2

A. Schematic drawing of Mg^{++} isocitrate bound in the active site of IDH. Hydrogens are shown for illustrative purposes where hydrogen bonds between enzyme and substrate are thought to occur. Dashed lines indicate likely hydrogen bonds or salt bridges. Water molecules are not shown.

Figure 3

A. Structures of substrate-bound IDH (solid bonds) and phosphorylated IDH (open bonds). B. Structures of substrate-bound S113E (open bonds) and wild-type IDH (solid bonds), showing the movements of the γ-carboxylate of isocitrate.

Crystallographic Statistics

Space Group: $P4_32_12$ Cell Dimensions: a=b=105.1 Å c=150.3 Å

	Unique Reflections Possible	Unique Reflections Collected	Observations Collected	Refl.s Used in Refinement	Rmerge
Mg complex	30274	29506	111257	19414	0.144*
Mn complex	30274	13048	31102	---	0.094
S113D free	21721	20711	89070	12774	0.204*
S113E free	34306	27716	67344	19209	0.099
S113E complex	30274	26412	62251	18367	0.093

	Rcryst	rms Δbond	rms Δangle	Resolution
Mg complex	0.176	0.019 Å	3.4°	2.5 Å
S113D free	0.163	0.016 Å	3.3°	2.8 Å
S113E free	0.179	0.016 Å	3.1°	2.4 Å
S113E complex	0.168	0.016 Å	3.1°	2.5 Å

Electrostatic Potential Changes at Substrate

$\Delta\Phi$ (kcal/mole·e)

atom	xtal	A	B	C	D
O1	-2.2	-3.0	-1.0	-1.3	-2.1
O2	-1.9	-2.6	-1.1	-1.2	-2.0
O3	-7.6	-3.1	-2.0	-2.7	-6.8
O4	-25.4	-2.1	-5.2	-5.2	-13.0
O5	-3.9	-5.7	-2.4	-2.0	-3.7
O6	-3.9	-5.9	-3.3	-2.4	-5.1
Mg	-1.2	-1.8	-0.8	-1.0	-1.6

$\Delta(\Delta G_{bind})$ (kcal/mole)

	xtal	A	B	C	D
	21.0*	7.5	5.8	5.4	13.1

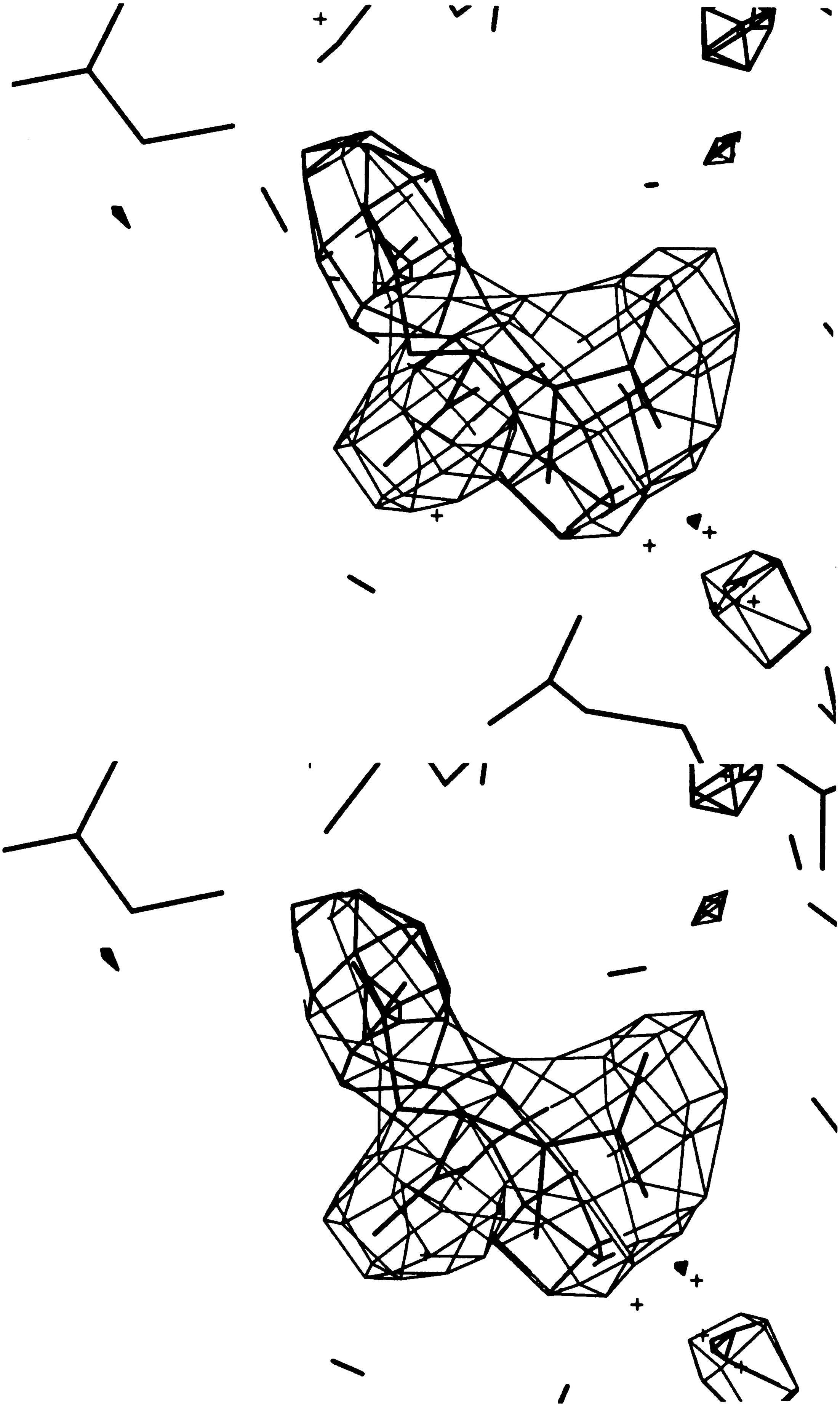

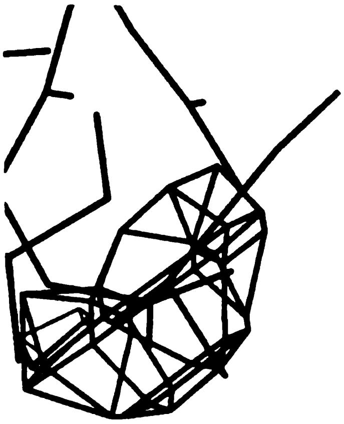

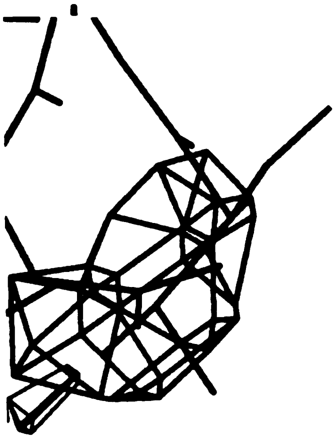

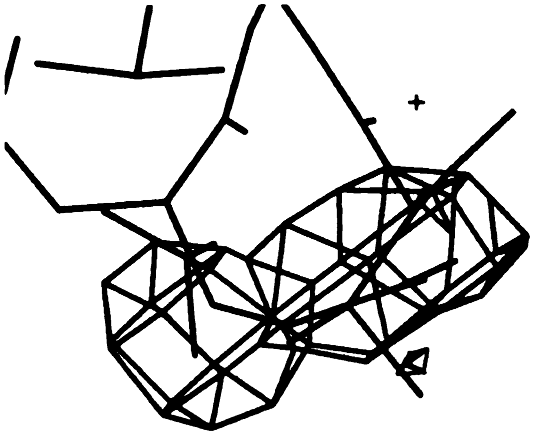

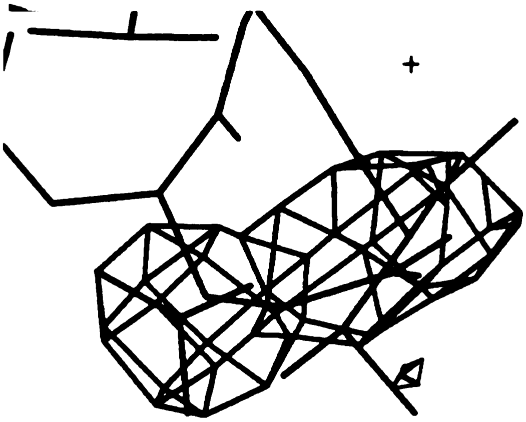

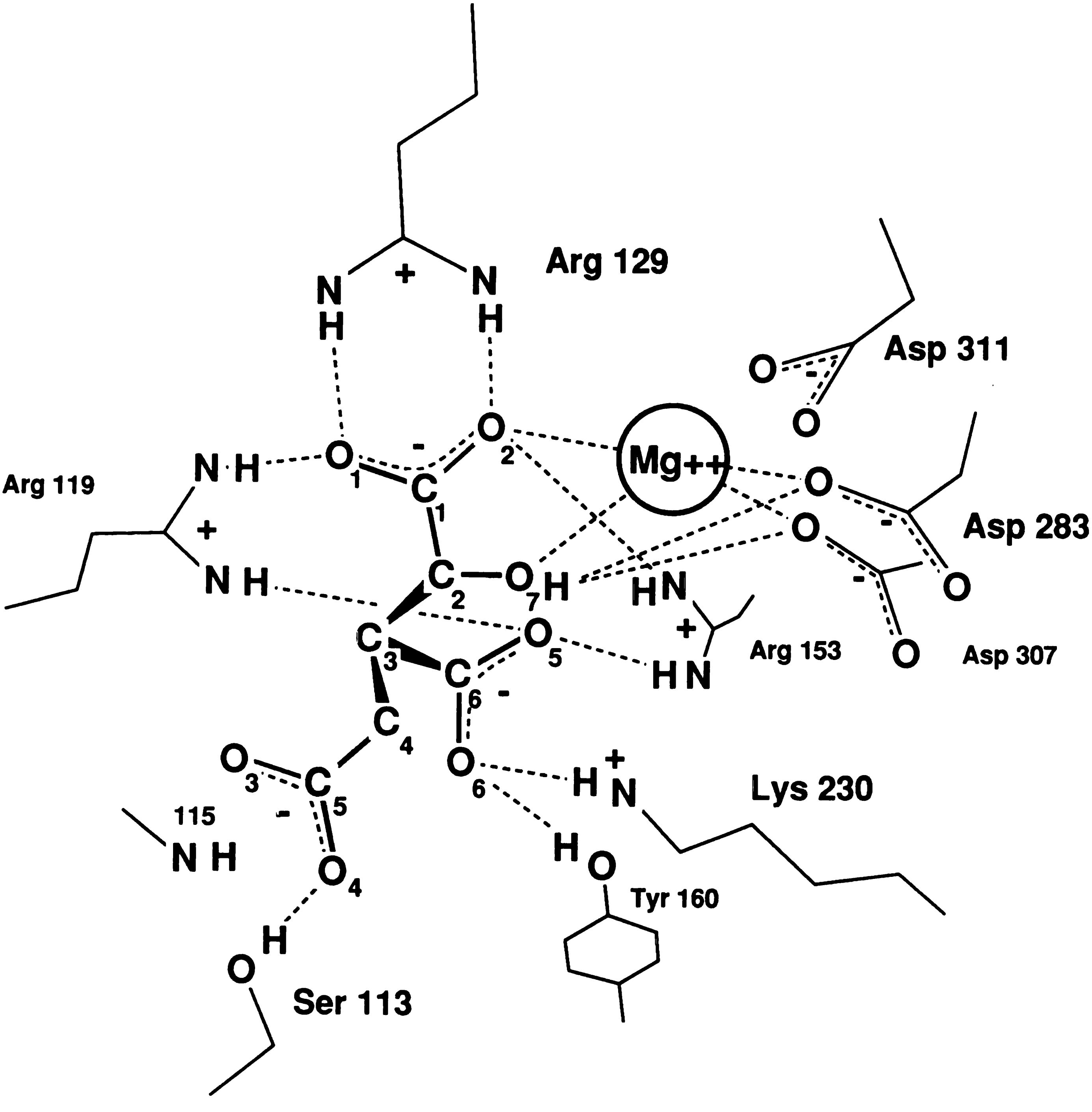
Arg 129
N H
+
N H
Asp 311
O
-
O
Arg 119
N H
O1
-
C1
O2
Mg++
O
-
Asp 283
+
N H
C2
O7 H
O
-
O
HN
+
Arg 153
O
Asp 307
C3
C6
O5
HN
-
C4
O3
C5
-
115
N H
O4
O6
H
+
N
Lys 230
H
O
Tyr 160
H
O
Ser 113

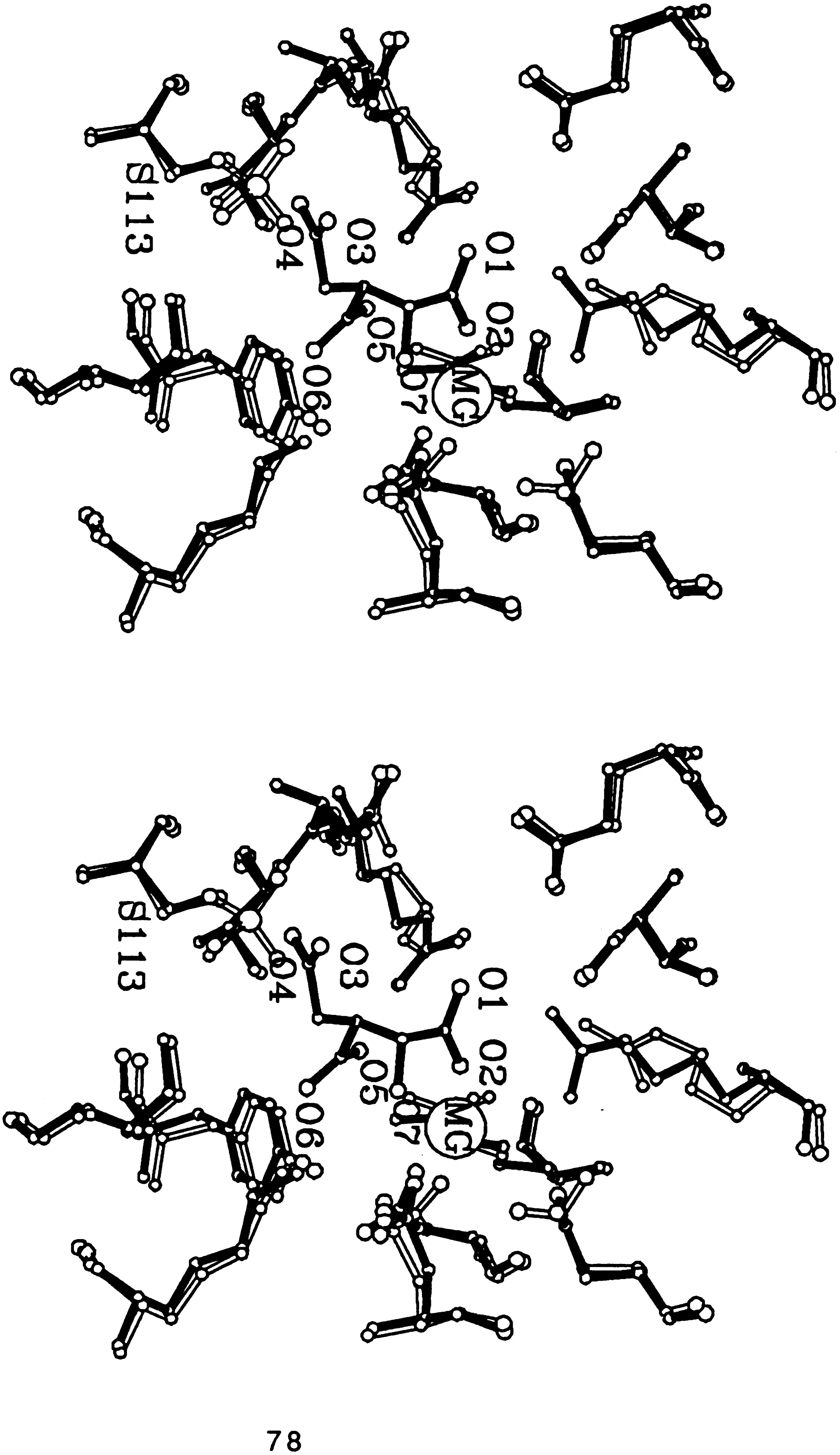
S113
O4
O3
O1
O2
O5
O6
O7
MG

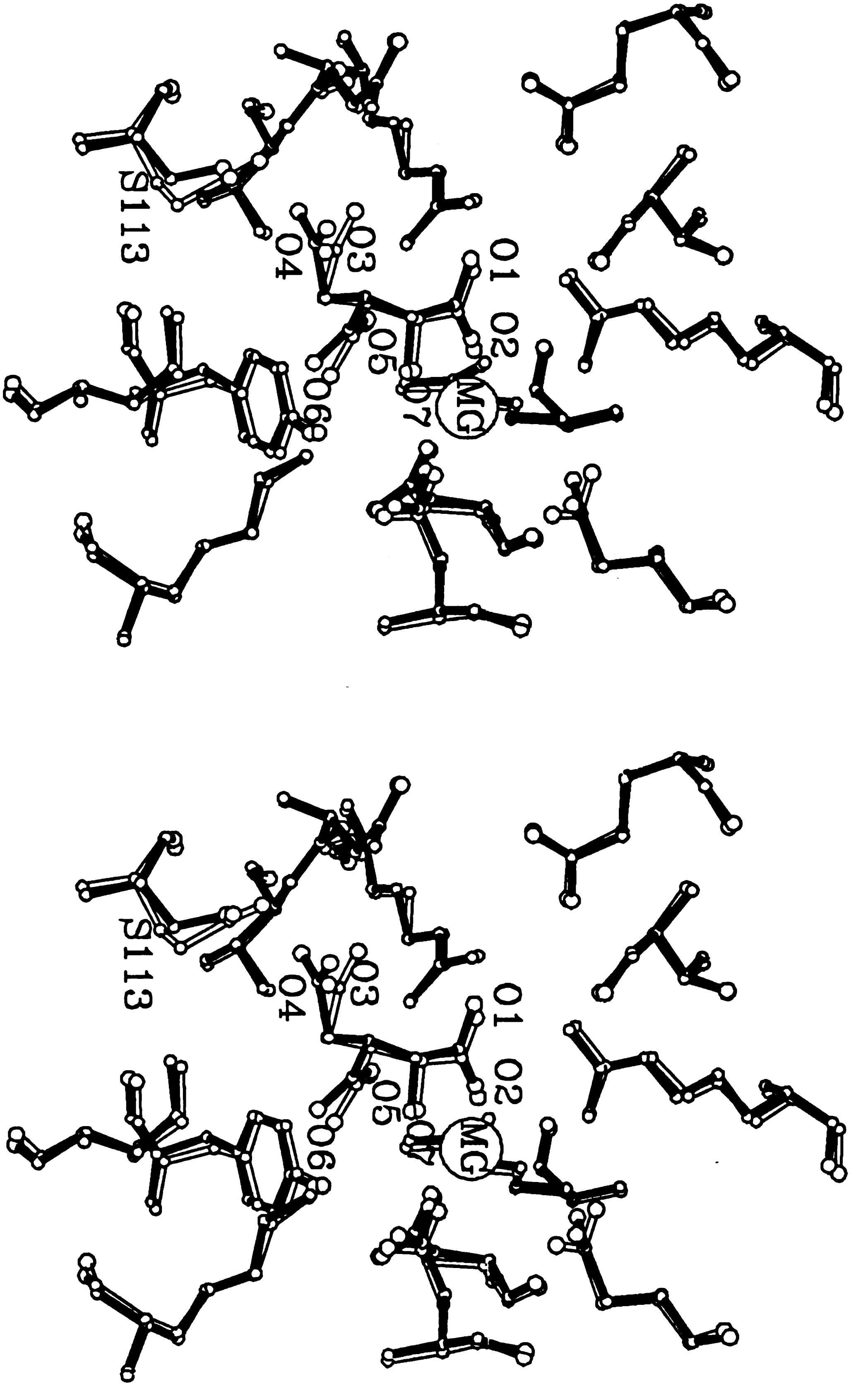
S113
O4
O3
O1
O2
O5
O6
O7
MG

Catalytic mechanism of isocitrate dehydrogenase: structure of a magnesium-isocitrate ternary complex

James H. Hurley[†], Antony M. Dean[§], Daniel E. Koshland, Jr.[§], and Robert M. Stroud[†¶]

[†]Department of Biochemistry and Biophysics and Graduate Group in Biophysics
University of California
San Francisco, Ca. 94143-0448

[§]Department of Biochemistry
University of California
Berkeley, Ca. 94720

¶. To whom correspondence should be addressed.

This work was supported by the National Institutes of Health GM 24485 to R.M.S. and the National Science Foundation 04200 to D.E.K., Pittsburgh Supercomputer Center DMB 890040P to R.M.S. for crystallographic refinement, and a University of California Regent's Fellowship to J.H.H. Atomic coordinates of the magnesium-isocitrate complex with isocitrate dehydrogenase have been deposited at the Brookhaven Protein Data Bank.

The structure of magnesium and isocitrate bound to isocitrate dehydrogenase has been determined at 2.5 Å resolution by the Fourier difference technique and refined to an R-factor of 17.6 %. The metal ion is coordinated to the α-carboxylate and hydroxyl oxygen (O7) of isocitrate in a manner suitable for stabilization of the formation of a negative charge on O7 during both dehydrogenation and decarboxylation steps of the conversion of isocitrate to α-ketoglutarate. The metal ion is also coordinated by aspartate side chains 283' (' indicates the second subunit of the dimer) and 307 and two water molecules in a roughly octahedral arrangement. Based on the geometry of the active site, the base functioning in the dehydrogenation step is most likely aspartate 283'. The active site acid responsible for protonation of C3 of the enolate form of α-ketoglutarate after the decarboxylation step may be one to the amino acids hydrogen bonded to the β-carboxylate of isocitrate, tyrosine 160 or lysine 230'. The observation that the α, β, and hydroxyl moieties, common to isocitrate and isopropylmalate, are bound by residues identical in both sequences confirms the common evolutionary origin of the substrate binding sites of isocitrate dehydrogenase and isopropylmalate dehydrogenase.

Isocitrate dehydrogenase (*threo*-Ds-isocitrate-NAD(P)+ oxidoreductase [decarboxylating], E.C. 1.1.1.42) (IDH) catalyzes the oxidation and decarboxylation of isocitrate to α-ketoglutarate, a step in the citric acid cycle. The reaction occurs in two steps (1):

$$\text{isocitrate} + \text{NAD(P)}^+ \text{ -- > oxalosuccinate} + \text{NAD(P)H} + \text{H}^+$$

$$\text{oxalosuccinate} + \text{H}^+ \text{ --> } \alpha\text{-ketoglutarate} + \text{CO}_2$$

$NADP^+$-dependent IDH requires Mg^{++}, or a transition metal such as Mn^{++} or Cd^{++} for activity. Here we discuss the catalytic mechanism of this enzyme in light of the three-dimensional structure of a Mg^{++} isocitrate complex (2) with the $NADP^+$-dependent IDH of *Escherichia coli*, a dimer of identical 416-amino acid subunits.

In the first step of the IDH reaction, the dehydrogenation step, a proton is removed from the hydroxyl oxygen and a hydride is transferred to $NADP^+$. A base is expected to abstract the proton from the hydroxyl group. The pH profile for inhibition by the competitive inhibitor of IDH oxalylglycine (3) demonstrates a pK_i of 5.7, suggesting the presence of an active site base titrating at this pH. The best-characterized dehydrogenases feature electrostatic stabilization of the negative charge which develops on the hydroxyl oxygen in the transition state. Electrostatic catalysis may be mediated either by an amino acid residue, such as arginine 109 in lactate dehydrogenase (4), or a metal ion, such as Zn^{++} in alcohol dehydrogenase (5). The identities of the groups involved in electrostatic and base catalysis are central questions for elucidation of the IDH mechanism.

In the second step of the IDH reaction, oxalosuccinate is decarboxylated to α-ketoglutarate by removal of the β-carboxylate. CO_2, rather than HCO_3^-, is the immediate product of decarboxylation (6). It has long been believed that Mg^{++}-dependent enzymatic β-decarboxylation of α-ketoacids is similar to the Mg^{++}-catalyzed reaction in solution. In a study of model compounds, the nonenzymatic β-decarboxylation of dimethyloxaloacetic acid and its ester demonstrated divalent metal ion catalysis in solution for the carboxylic acid reaction, but not for the ester (7). It was thus proposed that the metal ion was coordinated by the keto oxygen and the adjacent α-carboxylate, and stabilized the formation of an enolate intermediate.

There is substantial spectroscopic and kinetic evidence in support of the key role of the metal ion for $NADP^+$-linked IDH. EPR and ultrafiltration binding studies of pig heart showed a 20-fold decrease in the Kd for Mn^{++} in the presence of isocitrate, indicating that the principal substrate was the metal-isocitrate complex (8), and suggesting coordination of the metal ion by isocitrate on the enzyme. The ESR resonances for Mn^{++} changed markedly in the presence of IDH, with a further change on addition of isocitrate, further evidence for direct metal-isocitrate coordination on the enzyme (9). Multinuclear NMR spectra for enzyme-bound ^{113}Cd in the presence of isocitrate are characteristic of coordination by six oxygen ligands (10). Distances from a proton relaxation study of Mn^{++}-isocitrate in solution were consistent with bidentate chelation of the metal by the α-carboxylate and hydroxyl oxygen, although direct data for the enzyme-bound complex could not be obtained (11). ^{13}C NMR results also showed that enzyme-bound isocitrate is fully ionized (12). The kinetics of the $NADP^+$-linked IDH of *Salmonella typhimurium* (13), closely related to *E. coli*, demonstrated that the metal isocitrate complex is the kinetically important substrate, and suggested that the mechanisms of prokaryotic and eukaryotic $NADP^+$-linked IDH are likely to be similar. Despite extensive spectroscopic information on the role of the metal ion, to date there has been no direct evidence that the metal ion is coordinated by the α-carboxylate and hydroxyl oxygen of isocitrate on the enzyme.

^{13}C NMR resonances characteristic of the enol form of enzyme-bound α-ketoglutarate have been observed (12), direct evidence for the presence of this intermediate. IDH catalyzes the stereospecific exchange of the β-hydrogen (14), evidence that an acidic group on the enzyme protonates the enol form of α-ketoglutarate prior to dissociation. The identity of this group is another key question regarding the IDH mechanism.

The overall enhancement of metal-catalyzed decarboxylation by an enzyme has been estimated from isotope effect experiments. The observation of a ^{13}C isotope effect for the non-enzymatic reaction, but not for the enzymatic reaction, suggested that for the decarboxylation of oxaloacetate, the enzyme accelerates carbon-carbon bond scission by roughly a factor of 10^8 (15). The ^{13}C isotope effect for the decarboxylation of oxalosuccinate by IDH at neutral pH is barely measurable (3), suggesting a large acceleration in rate for this step in IDH. Based on the pH dependence of the ^{13}C isotope effect, substrate dissociation is 16-fold slower than catalysis. The overall rate acceleration thus less than the rate acceleration for the carbon-carbon bond scission step.

IDH, malic enzyme, and isopropylmalate dehydrogenase (IMDH) belong to a class of metal ion-dependent decarboxylating dehydrogenases which catalyze essentially identical reactions for isocitrate, malate, and isopropylmalate, respectively. Sequences of IDH and IMDH are 25-29 % identical for aligned residues (16,17). There is no apparent sequence similarity with L-malic enzyme (18,19). Although D-malate is not the common biological form, there is an inducible D-malic enzyme in *E. coli* (20). The absolute configuration of the biological isomer of isocitrate is R at C_β (21), as is the absolute configuration of D-malate. The absolute configuration at C_β is almost certainly R for isopropylmalate as well, as D-malic enzyme shows some activity with this substrate (20). The evolutionary relationship of these two α-R hydroxyacid decarboxylating dehydrogenases IDH and IMDH may be investigated by comparison of residues found in the active site of IDH with IMDH sequences.

Experimental Procedures

IDH crystals (17) were soaked in ligand-containing solutions . IDH crystals were soaked for at least three hours in freshly prepared solutions of 100 mM *threo*-Ds(+)-isocitric acid (monopotassium salt) obtained from Sigma, 10 mM of either $MgSO_4$ or $MnCl_2$, 100 mM NaCl, 35 mM Na_2HPO_4, 2 mM DTT and 0.02 % NaN_3 in 50 % saturated $(NH_4)_2SO_4$, with pH adjusted to

6.0 with concentrated NH_4OH. In order to unambiguously determine the metal binding site by Fourier difference mapping, x-ray reflection data were collected as previously described (17) to 2.5 Å resolution both for crystals soaked in Mg^{++} and Mn^{++} containing solutions. The metal ion was located in the largest peak (11 σ) in an $(F_o(Mn)-F_o(Mg))\alpha_{calc}$ Fourier difference map (Fig. 1), with phases calculated from the refined structure of unliganded dephosphorylated IDH. Local scaling was used for all map calculations. The 11 σ peak in the $(F_o(Mn)-F_o(Mg))\alpha_{calc}$ difference map coincided with the largest peak (18 σ) in an $(F_o(Mn)-F_o(Free))\alpha_{calc}$ difference map and a major peak in an $(F_o(Mg)-F_o(Free))\alpha_{calc}$ difference map. $(F_o(Mn)-F_o(Free))\alpha_{calc}$ and $(F_o(Mg)-F_o(Free))\alpha_{calc}$ difference maps showed a large negative peak (-16 σ) at water 417 in the unliganded structures. This indicated that molecule 417, which is modeled reasonably as a water, but could also be some other species (ammonium, sodium, chloride, phosphate, and citrate are present in the soaking solution for unliganded crystals), was displaced in the liganded enzyme. Because of the displacement of water 417, which resulted in negative difference density in part of the region where isocitrate was believed to bind, the $(F_o(Mg)-F_o(Free))\alpha_{calc}$ difference map was not useful for placing isocitrate. Water 417 was removed and the Mg^{++} ion was placed at the major peak in the $(F_o(Mn)-F_o(Mg))\alpha_{calc}$ Fourier difference map. An R-factor of 0.239 was calculated with respect to Mg isocitrate amplitudes for this model prior to refinement. Reflections with $F/\sigma(F)>1.0$ were used in refinement and R-factor calculation. This model was then refined with XPLOR minimization (22) to an R-factor of 0.184. Energy parameters were obtained from the CHARMM library (23) normally used with XPLOR, except van der Waals parameters were added for Mg^{++} and improper angles for the two chiral centers of isocitrate were calculated from the small molecule structure (21). An $(F_o(Mg)-F_c)\alpha_{calc}$ difference map (Fig. 2) with amplitudes and phases calculated from the refined Mg complex model allowed unambiguous placement of R,S-isocitrate, the biologically relevant isomer (21). After including isocitrate, the model was refined to a final R-factor of 0.176 (Table 1).

Results

Isocitrate binds in the pocket between the large and small domains of IDH (Fig. 3), referred to as the "front pocket" (17). Hydrogen bonds are formed between isocitrate and serine 113, arginines 119, 129, and 153, tyrosine 160, lysine 230' (where ' denotes the second subunit), and waters 458, 479, 560, 561, and 562 (Table 2, Fig. 4). Asparagine 115, with an N_δ - O4 distance of 3.4 Å, probably interacts electrostatically with isocitrate but does not form a hydrogen bond. Waters 458 and 479 are present in the unliganded structure of IDH (there are water molecules within 1 Å of these in the superposed structures); waters 560-562 are unique to the substrate-bound structure. Isocitrate is bound in a partially folded conformation; the C1-C2-C3-C4 and C2-C3-C4-C5 torsion angles are -165^o and 107^o, with the γ-carboxylate closer to the α-carboxylate than in the extended conformation found in the small molecule structure of the potassium salt of isocitrate, -166^o and 150^o.

Mg^{++} is directly coordinated by the α-carboxylate and hydroxyl oxygen of isocitrate, and coordinated by a total of six oxygen ligands in a roughly octahedral arrangement (Fig. 5). Two ligands are contributed by isocitrate, O2 of the α-carboxylate and the hydroxyl O7. Two are provided by the side chains of aspartates 283' and 307, and two by water molecules 458 and 562. Mg^{++} is relatively well-ordered, with B = 27, as are the two Mg^{++}-bound water molecules 458 and 562, with B = 24 and 28 respectively. Aspartate 311 is a second-nearest neighbor, 3.5 Å from the metal.

There are significant local structural changes in the enzyme on substrate binding (Fig. 6) . A rotation of the side chain of arginine 129 moves the guanidino group by up to 2.1 Å. Arginine 119 also rotates, but with a net movement of the guanidino group by at most 0.5 Å. The Nε of lysine 230 moves 0.7 Å, and tyrosine 160 rotates, moving the hydroxyl oxygen 0.9 Å. The side chain of aspartate 311 moves up to 1.3 Å, while the two aspartates directly coordinating Mg^{++} move by no more than 0.4 Å. The rms shift for all main chain atoms (including C_β) between the two structures is 0.25 Å. This is less than the estimated mean coordinate error of 0.4 Å in either structure (24), which is expected as the structures were not independently determined. No significant structural changes are seen far from the isocitrate binding site (Fig. 7).

Discussion

The geometry of the Mg^{++} isocitrate complex provides direct confirmation of the key role of the metal ion. The Mg^{++} is in a position to stabilize the negative charge which develops on the hydroxyl oxygen during oxidation of C2 during the dehydrogenation reaction. The second step of the reaction, decarboxylation at C3, is also catalyzed by stabilization of a negative charge which develops at the same oxygen for the enolate form of α-ketoglutarate. Mg^{++}, which catalyzes the second step of the reaction in solution, appears to play the central role in transition state stabilization for both steps in the IDH reaction. As postulated by Steinberger and Westheimer (7), key roles of the enzyme are to determine substrate specificity and to enhance metal ion catalysis relative to the solution state. Metal-assisted decarboxylation is greatly enhanced by binding of the Mg^{++} isocitrate complex to the enzyme, but it is less clear how the enzyme promotes metal catalysis. Presumably the fixed charge distribution and inhomogeneous dielectric response in the active site stabilize charge rearrangements which are found in the transition state.

In addition to electrostatic catalysis, other roles for the enzyme are to lower the decrease in entropy of the transition state relative to isolated reactants by binding isocitrate and $NADP^+$ together, and to promote deprotonation at O7 and protonation at C3 by acid/base catalysis. A likely mechanism for the IDH reaction based on currently available knowledge is shown in figure 8. Given their proximity to O7, aspartates 283' and 307, and waters 560 and 562 are possible proton acceptors in the dehydrogenation step. If the base is the group which titrates at pH 5.7 in pig heart NADP+-dependent IDH, and if an analogous group is present in the *E. coli* IDH, the only candidates which remain are the two aspartates and water 562, which would have to exist as hydroxide at neutral pH. There are no other groups in the immediate vicinity of bound isocitrate which are likely to titrate near pH 5.7 except the metal-bound water molecule 458, which is not positioned to accept a proton directly from O7. Aspartate 283' is closest to O7, at 2.6 Å, and appears to be in a particularly favorable geometry for proton transfer. Protonation of aspartate 283' would be *syn*, which has been estimated to be up to 10^4 times more favorable than *anti* protonation (25).

The hydroxyl proton points directly away from Mg^{++} when positioned for transfer to the carboxylate group of this residue. Transfer to aspartate 307 or water 562 would require a closer approach of the proton to the metal ion, which would be sterically and electrostatically unfavorable. The close proximity of aspartate 283' to two other negatively charged side chains could account for the increase in the pKa from the intrinsic value for this residue. Definitive identification of the active site base, however, must await further experiments. In the second step of the IDH reaction it cannot be ruled out that α-ketoglutarate has a substantially different mode of binding from isocitrate which brings C3 closer to some now-unidentified proton donor. Tyrosine 160 and lysine 230', however, which are hydrogen-bonded to the β-carboxylate of isocitrate, are favorably positioned to serve as the acid catalyst which protonates C3 after decarboxylation.

Sequence comparison with IMDH reveals a consistent picture of the evolution of substrate specificity for the IDH-like class of decarboxylating dehydrogenases. All residues (119, 129, 153, 160, 230') interacting with the α, β, and hydroxyl moieties of isocitrate, which are common to isocitrate, isopropylmalate, and malate, are conserved between IDH and all known IMDH sequences. Residues interacting with the γ-carboxylate of isocitrate, 113 and 115, are unique to isocitrate and are not conserved with the IMDH sequences. The two aspartates 283' and 307 coordinating Mg^{++} are also conserved in all available sequences. Aspartate 311, a second-nearest neighbor to the metal, is conserved in all sequences except that of the extreme thermophile *Thermus thermophilus* (26), in which it is replaced by asparagine. There is no homology with the L-malic enzyme sequence, which is not unexpected given the opposite stereospecificities of the two enzymes. We expect it is likely that homologies will be found with the D-malic enzymes, yet to be sequenced. Given the topological dissimilarity of IDH to previously characterized dehydrogenases (17), the metal-dependent decarboxylating dehydrogenases appear to form a family evolutionarily distinct from other dehydrogenases.

Acknowledgements

We thank Joseph Villafranca, Roberta Colman, and Jim Remington for helpful discussions.

References

1. Siebert, G., Carsiotis, M. and Plaut, G.W.E. *J. Biol. Chem.* (1957) **226**:977-991.

2. Hurley, J. H., Dean, A. M., Sohl, J. L., Koshland, D. E., Jr., and Stroud, R. M. *Science* (1990) submitted.

3. Grissom, C.B. and Cleland, W.W. (1988) *Biochemistry* **27**:2934-2943.

4. Clarke, A. R., Wigley, D. B., Chia, W. N., Barstow, D., Atkinson, T. and Holbrook, J.J. (1986) *Nature* **324**:699-702.

5. Branden, C-.I., Jornvall, H., Eklund, H., and Furugren, B. in *The Enzymes* 3rd edn Vol. 11 (ed P.D. Boyer) 104-190 (Academic, New York 1975)

6. Londesborough, J.C. and Dalziel, K. (1968) *Biochem. J.* **110**:223 .

7. Steinberger, R. and Westheimer, F.H. (1951) *J. Am. Chem. Soc.* **73**:429-435.

8. Villafranca, J. J. and Colman, R.F. (1972) *J. Biol. Chem.* **247**:209-214.

9. Levy, R.S. and Villafranca, J.J. (1977) *Biochemistry* **16**:3293-3309.

10. Ehrlich, R.S. and Colman, R.F. (1989) *Biochemistry* **28**:2058-2065.

11. Villafranca, J.J. and Colman, R.F. (1974) *Biochemistry* **13**:1152-1160.

12. Ehrlich, R.S. and Colman, R.F. (1987) *Biochemistry* **26**:2461-3471.

13. Marr, J. J. and Weber, M. M. (1973) *Arch. Biochem. Biophys.* **158**:782-791.

14. Lienhard, G. E. and Rose, I.A. (1964) *Biochemistry* **3**:185-190.

15. Seltzer, S., Hamilton, G.A. and Westheimer, F.H. (1959) *J. Am. Chem. Soc.* **81**:4018-4024.

16. Thorsness, P. E. and Koshland, D. E., Jr. *J. Biol. Chem.* (1987) **262**:10422-10425.

17. Hurley, J.H. , Thorsness, P. E., Ramalingam, V., Helmers, N. H., Koshland, D.E., Jr., and Stroud, R.M. (1989) *Proc. Natl. Acad. Sci. USA* **86**:8635-8639.

18. Bagchi, S., Wise, L.S., Brown, M.L., Bregman, D., Sul, H.S. and Rubin, C.S. (1987) *J. Biol. Chem.* **262**:1558-1565.

19. Kobayashi, K., Doi, S., Negoro, S., Urabe, I. and Okada, H. (1989) *J. Biol. Chem.* **264**:3200-3205.

20. Stern, J.R. and Hegre, C.S. (1966) *Nature* **212**:1611-1612.

21. Van Der Helm, D., Pickworth, J.G., Johnson, C.K., Minkin, J.A., Burow, N.E. and Patterson, A.L. (1968) *Acta Crystallogr. Sect. B* **24**:578-592.

22. Brunger, A.T., Kuriyan, K., and Karplus, M. (1987) *Science* **235**:458.

23. Brooks, B.R., Broccoleri, R.E., Olafson, B.D., States, D.J., Swaminathan, S. and Karplus, M. (1983) *J. Comp. Chem.* **4**:187 .

24. Hurley, J. H., Dean, A. M., Thorsness, P. E., Koshland, D. E., Jr., and Stroud, R. M. *J. Biol. Chem.* (1990) In press.

25. Gandour, R. D. *Bioorganic Chemistry* (1981) **10**:169-176.

26. Kagawa, Y., Nojima, H., Nukiwa, N., Ishizuka, M., Nakajima, T., Yasuhara, T., Tanaka, T., and Oshima, T. (1984) *J. Biol. Chem.* **259**:2956-2960.

Table 1

Crystallographic statistics for complexes of IDH with Mg^{++} isocitrate and Mn^{++} isocitrate. The crystallographic R-factor, $Rc = \Sigma|F_o-F_c|/\Sigma F_o$ is summed over all reflections with $|F|/\sigma(F) > 1$ from 5 to 2.5 Å; F_o and F_c are the observed and calculated amplitudes. $R_{merge} = \Sigma|I_i-\langle I\rangle|/\Sigma\langle I\rangle$, summed over all observations to 2.5 Å. *Data was collected for only one Mn^{++} complex crystal; three crystals each were used for collection of the Mg^{++} data set.

Table 2

Distances of less than 3.5 Å to potential hydrogen-bonding or salt bridge-forming partners between isocitrate, metal, and enzyme. Atoms names used follow the Brookhaven protein data bank convention.

Figure 1

Divergent stereo view of the $(F_o(Mn)-F_o(Mg))\alpha_{calc}$ Fourier difference map at 2.5 Å resolution, contour level 5 σ, superimposed on the refined model of the Mg^{++} isocitrate complex.

Figure 2

Divergent stereo view of a $(F_o(Mg)-F_c)\alpha_{calc}$ difference map at 2.5 Å resolution with amplitudes and phases calculated from the refined Mg complex model, contour level 5 σ, superimposed on the refined model of the Mg^{++} isocitrate complex.

Figure 3

Divergent stereo view of the refined structure of the Mg^{++} isocitrate complex showing the active site. Both subunits are shown, with labelled residues belonging to the second subunit indicated by a primed number. Oxygen atoms of isocitrate are labelled following ref. 21, and the metal ion and residues involved in isocitrate and metal binding are identified. Except for three waters interacting with isocitrate or Mg^{++}, waters are not shown.

Figure 4

A schematic drawing of the active site of IDH. Hydrogens are shown for illustrative purposes where believed to participate in hydrogen bonds or salt bridges. Water molecules have been omitted for clarity. Residues belonging to the second subunit indicated by a primed number.

Figure 5

Divergent stereo view of the refined structure of the Mg^{++} isocitrate complex, showing the roughly octahedral coordination of the metal ion by substrate, bound water molecules, and aspartates 283' and 307.

Figure 6

Conformational changes on substrate binding are shown in this divergent stereo view of the active site. The substrate-bound structure is shown with solid bonds, the free enzyme with open bonds.

Figure 7

Mean atomic shift in Å between the substrate-bound and free forms of IDH, as a function of the distance of the atom in the substrate-bound structure from the nearest of the two bound isocitrate molecules in the dimer. Distances are measured from the C3 atom of isocitrate. The mean shift rapidly drops to the overall value by about 10 Å from the substrate. The scatter observed at large distances from the active site is probably due to the small number of atoms at these distances.

Figure 8

A likely mechanism for the reaction catalyzed by IDH. B is probably aspartate 283', and A is probably either tyrosine 160 or lysine 230'.

Crystallographic Statistics

Space Group: $P4_32_12$ Cell Dimensions: a=b=105.1 Å c=150.3 Å

	Unique Reflections Possible	Unique Reflections Collected	Observations Collected	Refl.s Used in Refinement	Rmerge
Mg complex	30274	29506	111257	19414	0.144*
Mn complex	30274	13048	31102	---	0.094

	Rcryst	rms Δbond	rms Δangle	Resolution
Mg complex	0.176	0.019 Å	3.4°	2.5 Å

Possible Hydrogen Bonds and Salt Bridges in the Mg^{++}-isocitrate Complex

O1	Arg 119 NH1	3.00
O1	Arg 129 NH1	3.01
O2	Arg 129 NH1	3.06
O2	Arg 153 NH2	2.92
O2	Water 458	3.04
O2	Mg	2.24
O4	Ser 113 OG	2.65
O4	Asn 115 ND	3.41
O5	Arg 119 NH2	2.81
O5	Arg 153 NH1	3.01
O6	Tyr 160 OH	2.80
O6	Lys 230' NZ	2.96
O7	Water 560	3.00
O7	Water 562	2.78
O7	Mg	1.92
O7	Asp 283' OD2	2.69
O7	Asp 307 OD2	2.92

Mg	Asp 283' OD2	2.34
Mg	Asp 307 OD2	2.09
Mg	Water 458	2.07
Mg	Water 562	1.86

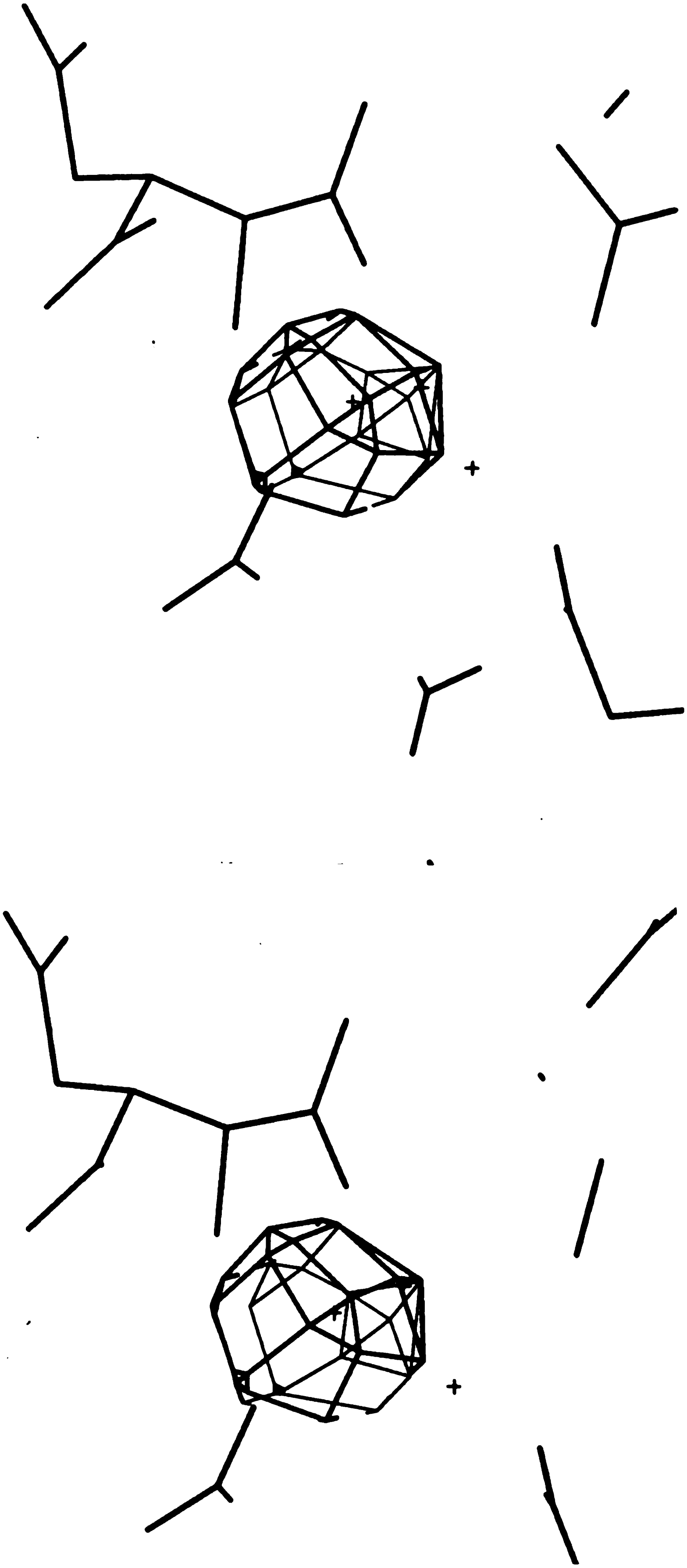

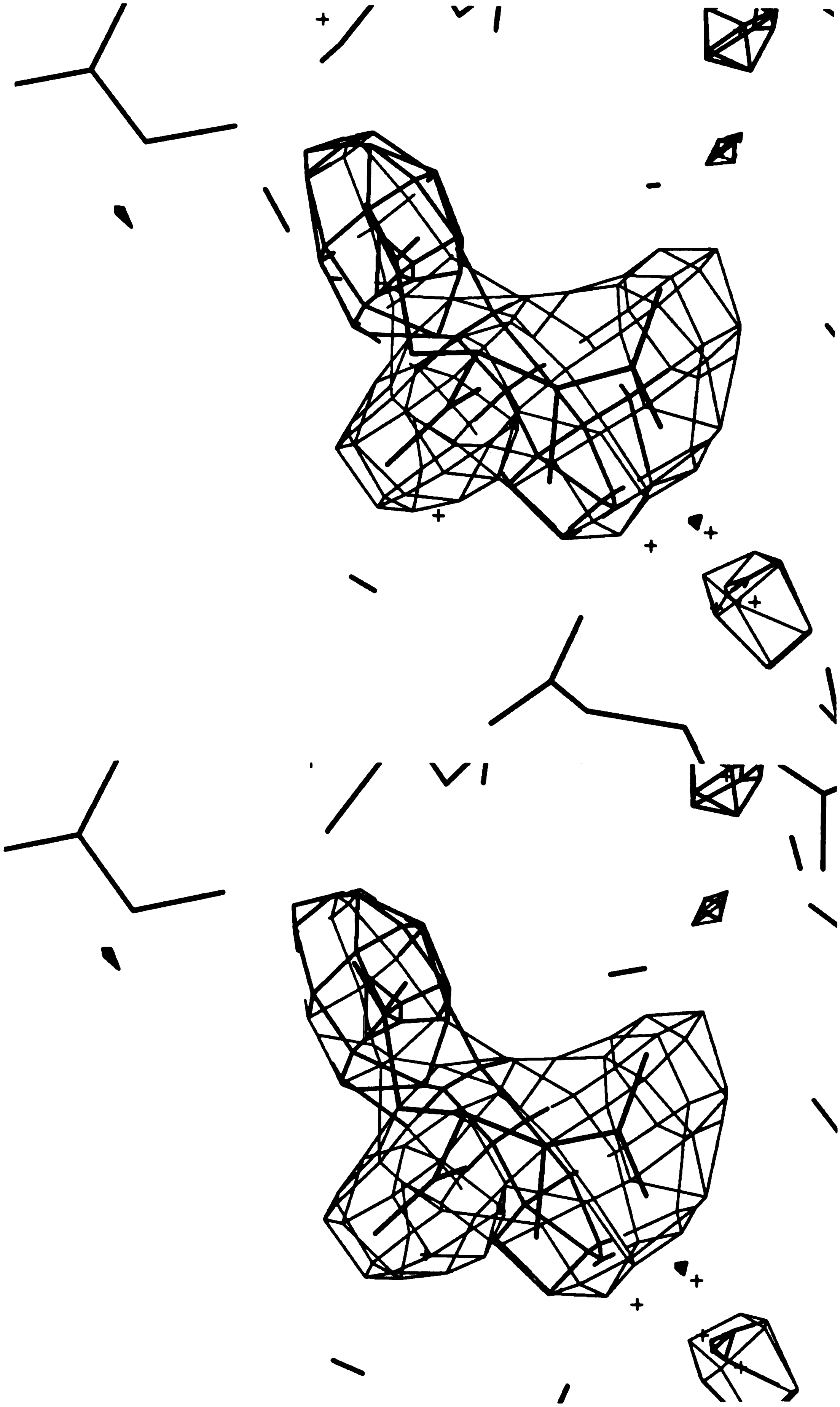

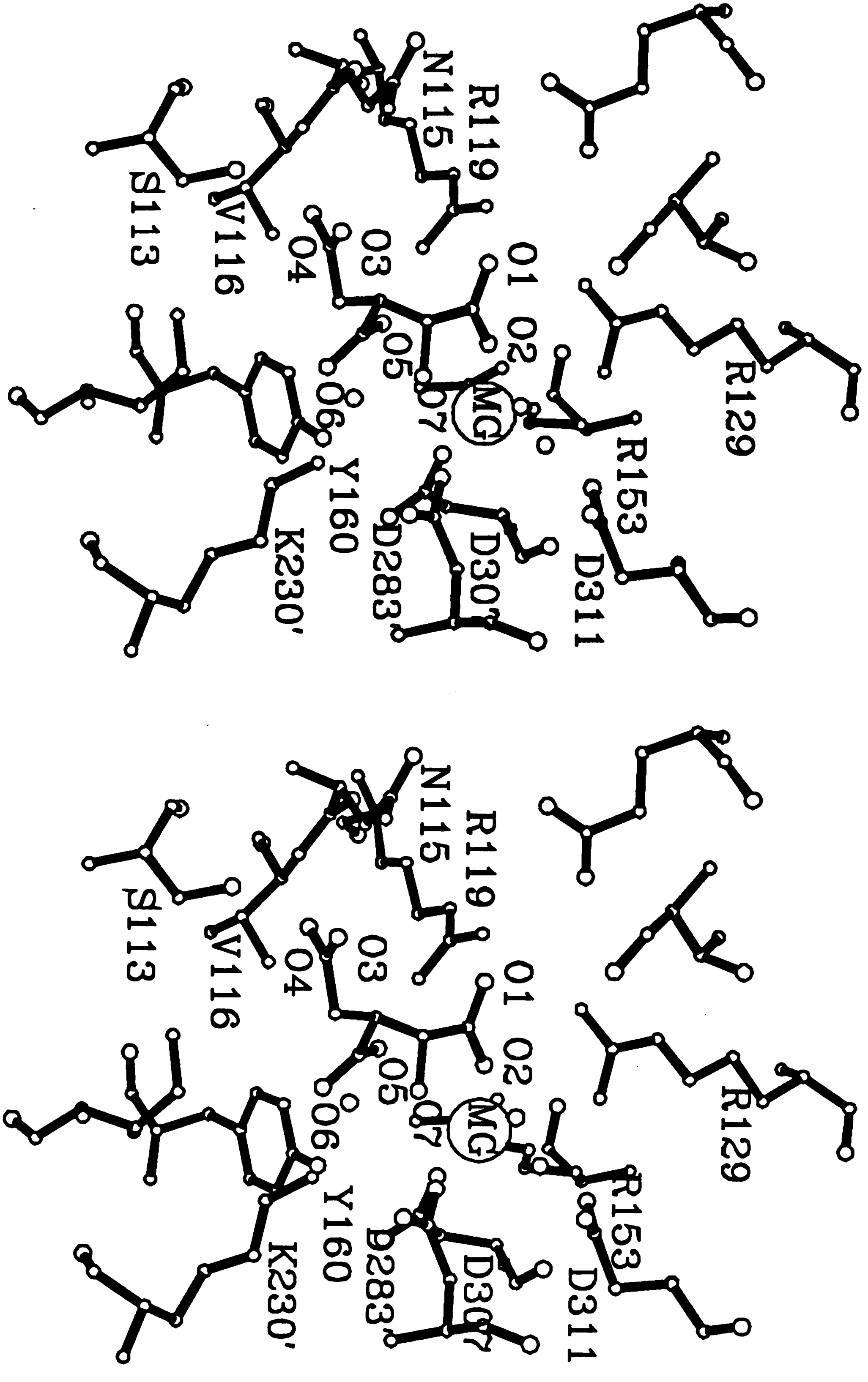
R129
R119
N115
S113
V116
O1
O2
O3
O4
O5
O6
O7
MG
R153
Y160
D311
D307'
D283'
K230'

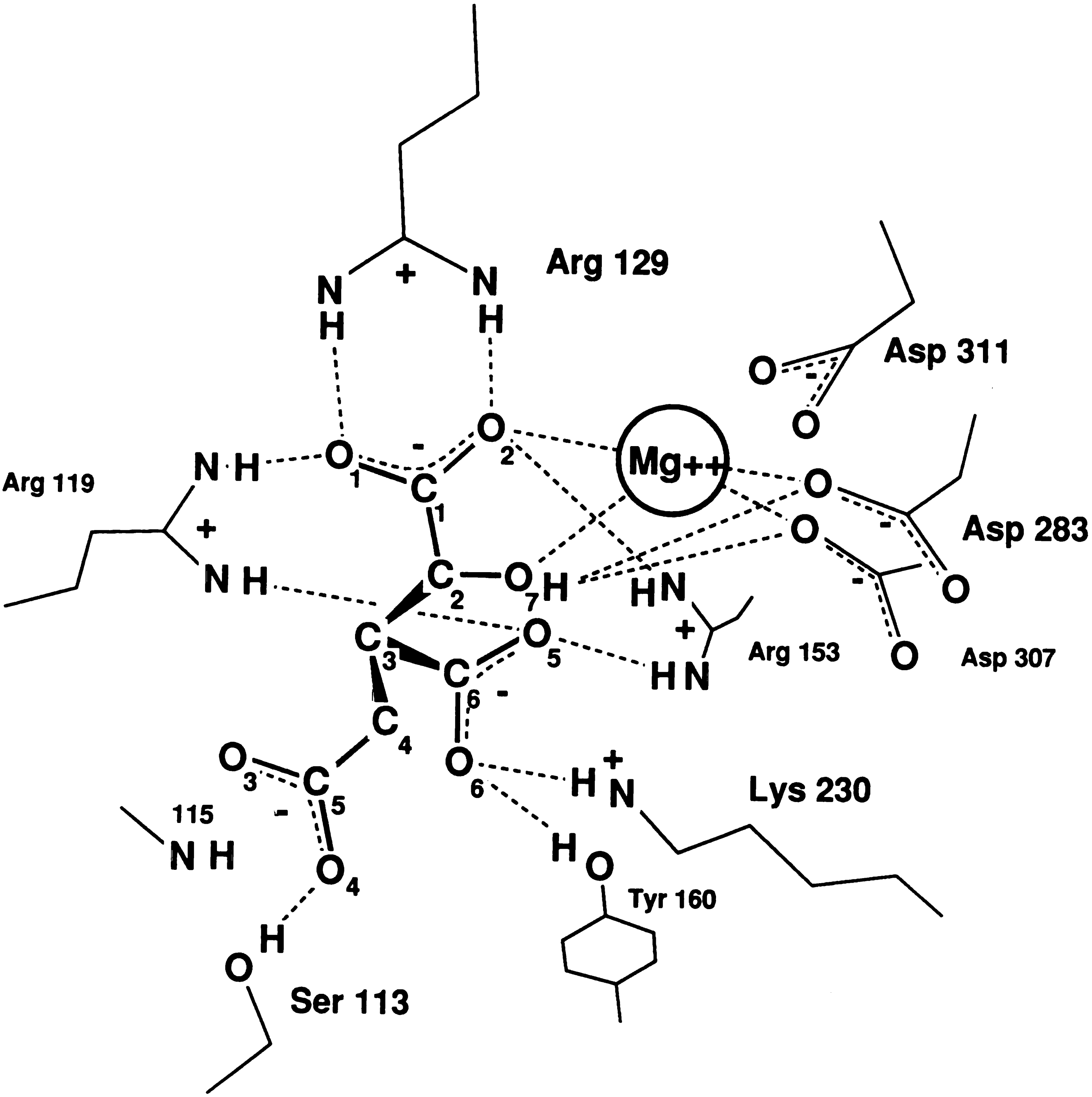
Arg 129
N
H
+
N
H
Asp 311
O
-
O
O
1
O
2
Mg++
O
Asp 283
-
O
Arg 119
N H
+
N H
C
1
C
2
O
7
H
O
-
O
HN
+
HN
Arg 153
O
Asp 307
C
3
O
5
C
6
-
C
4
O
3
C
5
-
O
6
H
+
N
Lys 230
115
N H
O
4
H
O
Tyr 160
H
O
Ser 113

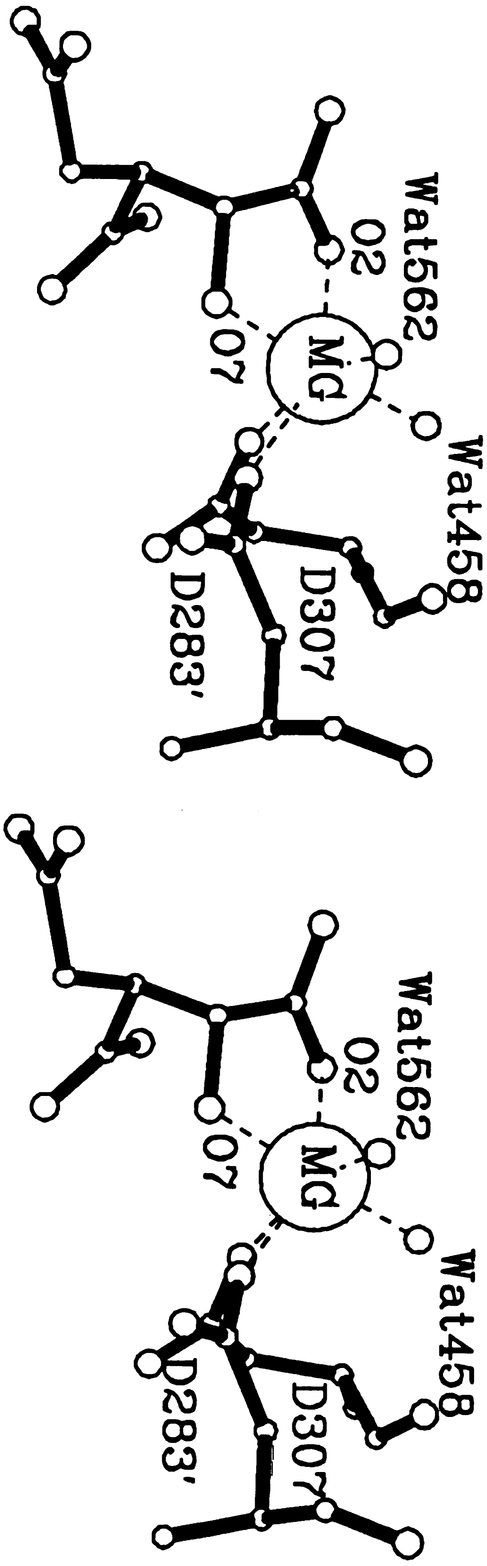
Wat562
O2
O7
MG
Wat458
D307
D283'

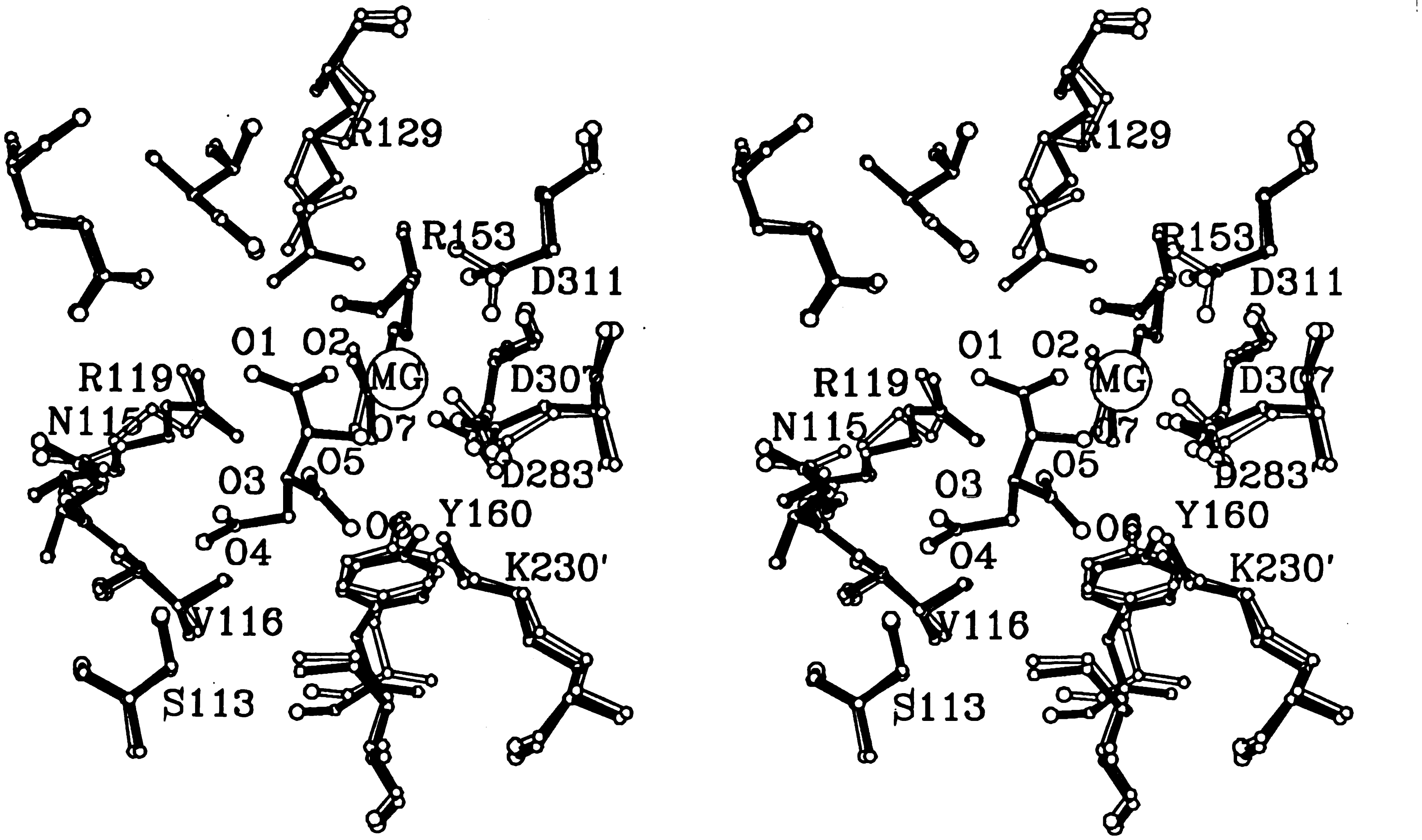
R129
R153
D311
O1
O2
MG
R119
D307
N115
O7
O5
D283'
O3
Y160
O6
O4
K230'
V116
S113

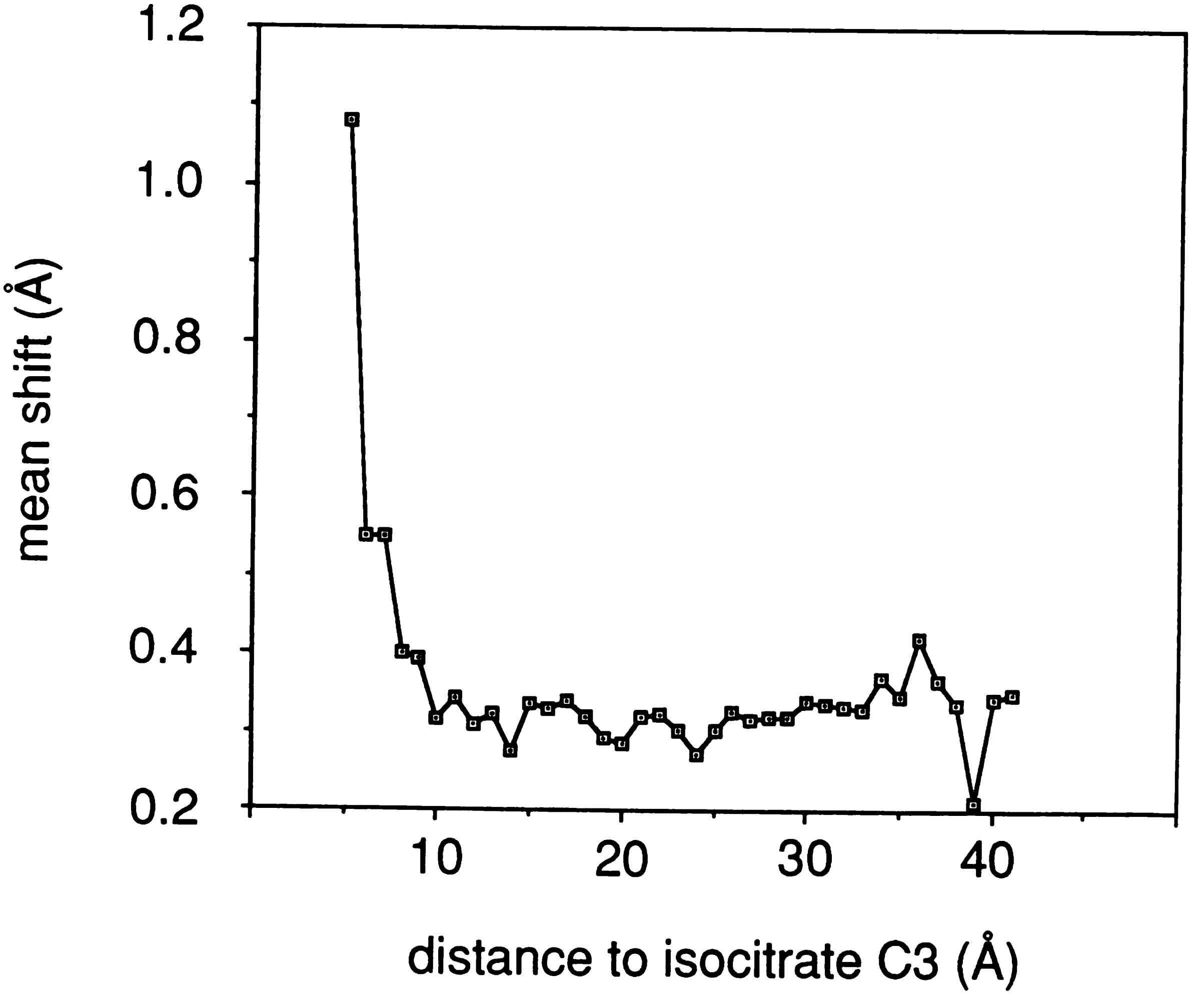
1.2
1.0
0.8
0.6
0.4
0.2
mean shift (Å)
10
20
30
40
distance to isocitrate C3 (Å)

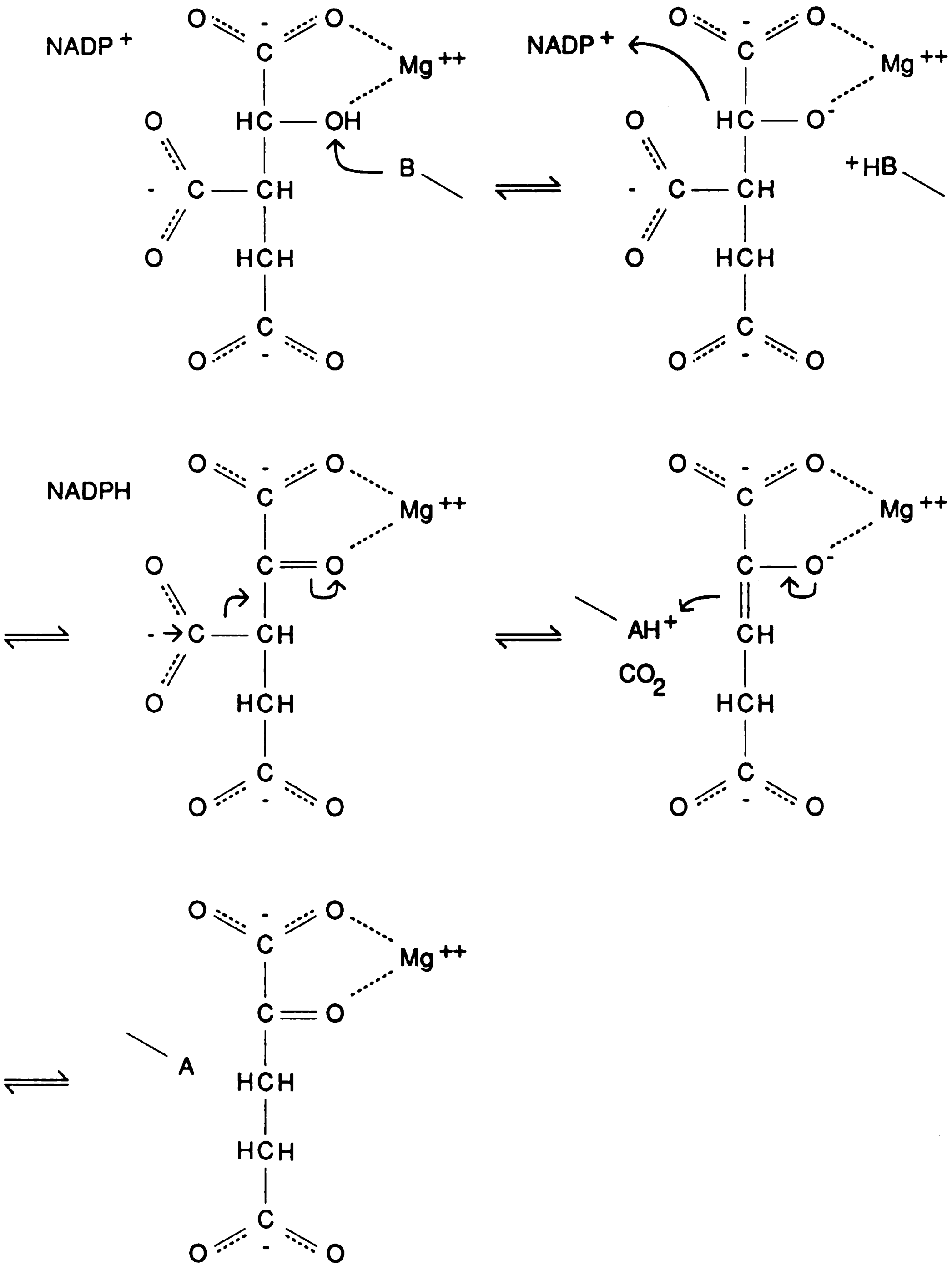
NADP +
Mg ++
B
NADP +
Mg ++
+ HB
NADPH
Mg ++
Mg ++
AH +
CO2
Mg ++
A

Conclusion

Study of IDH began in an effort to understand the most complex feature of living things: behavior. Specifically, how does a cell "know" how to modify its use of nutrients in response to changing external conditions ? Biochemistry has proved to be a most powerful approach to understanding biology, and in this case it was shown that the citric acid cycle could be slowed when IDH kinase/phosphatase phosphorylated IDH in response to allosteric control by a variety of metabolites, allowing the bacterial cell to grow on acetate. The science of biophysics arises from the origin of biological phenomena in the same physical laws that govern the inorganic world. Biophysics enters the picture when we are no longer satisfied with knowing which chemical reactions occur in cells, but want to know also the physical mechanisms by which reactions are catalyzed and by which they may be switched on or off. It was curiosity to understand the function of IDH at this more fundamental level that led to the structural studies.

IDH has proved to be a gratifyingly simple and elegant enzyme for a graduate student's thesis project. Because this enzyme is not regulated by a host of different allosteric effectors, I have been able essentially to complete the elucidation of the structural basis for regulation with the three structure determinations described in this thesis. The catalytic mechanism also appears relatively straightforward, and a complete mechanism can be proposed based on the structure of the enzyme-substrate complex and the kinetic and spectroscopic results of others. The physical and chemical reasoning connecting structure and function has been satisfyingly applied to both regulation and catalysis. One other major issue in the study of any enzyme is the question: how did it evolve ? The structural work has led to substantial new insights into the evolution of IDH, distinct from that of most familiar dehydrogenases, but closely related to that of isopropylmalate dehydrogenase.

Without having been entirely planned, the work on IDH seems to have fallen into the same pattern and addressed the same issues of regulation, catalysis, and evolution as the first pioneering crystallographic studies on enzymes: the "honorary enzyme" hemoglobin, lysozyme, carboxypeptidase A, chymotrypsin, trypsin, cytochrome C, lactate dehydrogenase. Although advances in technology have made such studies increasingly common, each enzyme has unique features, and appears to the crystallographer seeing a structure for the first time as a whole new world in miniature. In short, the process of obtaining the picture seen here for the structure and function of IDH has been a tremendously rewarding and informative experience.

The San Francisco
LIBRARY

FOR REFERENCE

NOT TO BE TAKEN FROM THE ROOM

BRO DART CAT. NO. 23 012 PRINTED IN U.S.A.